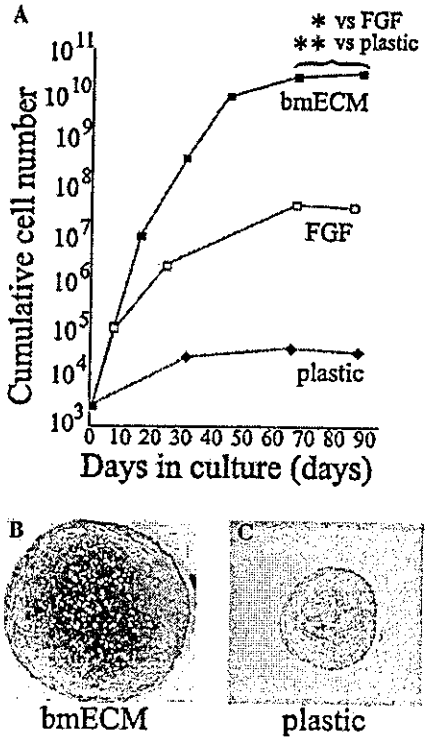

Fig. 3. Effects of bmECM on proliferation of MSC and their chondrogenic potential in cultures with human serum. (A) Human MSC, in the presence of 10% human serum, showed faster proliferation and a longer proliferative life span on bmECM than on plastic. Cells in marrow aspirates (1 ml/100-mm dish) from the ilium were seeded and maintained on plastic tissue culture dishes, as described in the legend of Fig. 1. The first passage was performed on plastic at a seeding density of 5000 cells/cm^2. In this study, MSC obtained from the 1st passage cultures on plastic were used for experimentation. The isolated cells were seeded on bmECM (endothelial) or on plastic as described in Materials and methods. FGF at 1 ng/ml was added to some cultures on plastic. *,**Differs significantly from the cell number in cultures on plastic dishes with FGF ("FGF") or without FGF ("plastic") on days 66–87 ($*p < 0.05$, $**p < 0.01$). The MSC from 66-day-old cultures on bmECM (B) or plastic (C) were transferred into the chondrogenic status in pellet cultures for 28 days and stained with toluidine blue.

bone, cartilage, and fat—are also in close contact with the basement membrane; satellite cells became myoblasts after detachment from the basal membrane [18]. These observations suggest that the basement membrane and/or some other ECMs play a crucial role in the proliferation of stem cells and the maintenance of their undifferentiated state. In this study, we showed that bmECM markedly increased both the growth rate and the proliferative life span of MSC. Furthermore, MSC that had expanded 10^6-fold on bmECM maintained its multi-lineage differentiation potential. The mechanism by which bmECM stimulates MSC proliferation and maintains their differentiation potential is not known, but even MSC transfected with telomerase gradually decreased its osteogenic potential with the increase in the passage number [5], although their replicative capacity was maintained. In contrast, MSC on bmECM maintained the differentiation potential even after they lost their replicative capacity. Thus, the extracellular matrix and telomerase may have complementary effects on the proliferation of MSC and their differentiation potential. In any case, the remarkable effects of bmECM in MSC cultures demonstrated here meet the expectations of doctors eager to expand MSC extensively in vitro from a small volume of marrow aspirates before transplantation. Henceforth, bmECM will be prepared using human ES or human cell lines, and in the near future bmECM-coated dishes will probably have a great use in MSC studies and regeneration medicine.

References

[1] M.F. Pittenger, A.M. Mackay, S.C. Beck, R.K. Jaiswal, R. Douglas, J.D. Mosca, M.A. Moorman, D.W. Simonetti, S. Craig, D.R. Marshak, Multilineage potential of adult human mesenchymal stem cells, Science 284 (1999) 143–147.

[2] R.J. Deans, A.B. Moseley, Mesenchymal stem cells: biology and potential clinical uses, Exp. Hematol. 28 (2000) 875–884.

[3] S. Tsutsumi, A. Shimazu, K. Miyazaki, H. Pan, C. Koike, E. Yoshida, K. Takagishi, Y. Kato, Retention of multilineage differentiation potential of mesenchymal cells during proliferation in response to FGF, Biochem. Biophys. Res. Commun. 288 (2001) 413–419.

[4] A. Muraglia, R. Cancedda, R. Quarto, Clonal mesenchymal progenitors from human bone marrow differentiate in vitro according to a hierarchical model, J. Cell Sci. 113 (2000) 1161–1166.

[5] S. Shi, S. Gronthos, S. Chen, A. Reddi, C.M. Counter, P.G. Robey, C.Y. Wang, Bone formation by human postnatal bone marrow stromal stem cells is enhanced by telomerase expression, Nat. Biotechnol. 20 (2002) 587–591.

[6] A. Oohira, T.N. Wight, J. McPherson, P. Bornstein, Biochemical and ultrastructural studies of proteoheparan sulfates synthesized by PYS-2, a basement membrane-producing cell line, J. Cell Biol. 92 (1982) 357–367.

[7] B. Tyree, E.A. Horigan, D.L. Klippenstein, J.R. Hassell, Heterogeneity of heparan sulfate proteoglycans synthesized by PYS-2 cells, Arch. Biochem. Biophys. 231 (1984) 328–335.

[8] J.R. Couchman, A. Woods, M. Hook, J.E. Christner, Characterization of a dermatan sulfate proteoglycan synthesized by murine parietal yolk sac (PYS-2) cells, J. Biol. Chem. 260 (1985) 13755–13762.

[9] D. Gospodawowicz, A.L. Mesher, C.R. Birdwell, Stimulation of corneal endothelial cell proliferation in vitro by fibroblast and epidermal growth factors, Exp. Eye Res. 137 (1977) 15–23.

[10] D. Gospodarowicz, R. Gonzalez, D.K. Fujii, Are factors originating from serum, plasma, or cultured cells involved in the growth-promoting effect of the extracellular matrix produced by cultured bovine corneal endothelial cells? J. Cell. Physiol. 114 (1983) 191–202.

[11] A. Martinez-Hernandez, A.E. Chung, The ultrastructural localization of two basement membrane components: entactin and laminin in rat tissues, J. Histochem. Cytochem. 32 (1984) 289–298.

[12] E. Hahn, G. Wick, D. Pencev, R. Timpl, Distribution of basement membrane proteins in normal and fibrotic human liver: collagen type IV, laminin, and fibronectin, Gut 21 (1980) 63–71.

[13] R.W. Farndale, C.A. Sayersm, A.J. Barrett, A direct spectrophotometric microassay for sulfated glycosaminoglycans in cartilage cultures, Connect. Tissue Res. 9 (1982) 247–248.
[14] O.A. Bessey, O.H. Lowry, O.H. Brock, A method for the rapid determination of alkaline phosphatase with five cubic millimeters of serum, J. Biol. Chem. 164 (1946) 321–329.
[15] H.J. Gitelman, An improved automated procedure for the detemination of calcium in biological specimens, Anal. Biochem. 18 (1967) 521–531.
[16] W. Guo, J.K. Choi, J.L. Kirkland, B.E. Corkey, J.A. Hamilton, Esterification of free fatty acids in adipocytes: a comparison between octanoate and oleate, Biochem. J. 349 (2000) 463–471.
[17] P. Kaur, A. Li, Adhesive properties of human basal epidermal cells: an analysis of keratinocyte stem cells, transit amplifying cells, and postmitotic differentiating cells, J. Invest. Dermatol. 114 (2000) 413–420.
[18] D.R. Campion, The muscle satellite cell: a review, Int. Rev. Cytol. 87 (1984) 225–251.

THE JOURNAL OF BIOLOGICAL CHEMISTRY

Vol. 278, No. 48, Issue of November 28, pp. 48259–48266, 2003
Printed in U.S.A.

Cystatin 10, a Novel Chondrocyte-specific Protein, May Promote the Last Steps of the Chondrocyte Differentiation Pathway*

Received for publication, November 14, 2002, and in revised form, September 15, 2003
Published, JBC Papers in Press, September 17, 2003, DOI 10.1074/jbc.M211639200

Yu Koshizuka‡, Takashi Yamada‡, Kazuto Hoshi§, Toru Ogasawara§, Ung-il Chung§, Hirotaka Kawano‡, Yusuke Nakamura¶, Kozo Nakamura‡, Shiro Ikegawa‖, and Hiroshi Kawaguchi‡****

From the Departments of ‡Orthopedic Surgery and §Tissue Engineering, Faculty of Medicine, and the ¶Laboratory of Molecular Medicine, Institute of Medical Science, University of Tokyo, Tokyo 113-8655 and the ‖Laboratory of Bone and Joint Diseases, SNP Research Center, Institute of Physical and Chemical Research, Tokyo 108-8639, Japan

This study attempts to characterize cystatin 10 (Cst10), which we recently identified as a novel protein implicated in endochondral ossification. Expression of Cst10 was specific to cartilage, localized in the cytosol of prehypertrophic and hypertrophic chondrocytes of the mouse growth plate. In the mouse chondrogenic cell line ATDC5, Cst10 expression preceded type X collagen expression and increased in synchrony with maturation. When we compared ATDC5 cells transfected with Cst10 cDNA with cells transfected with a mock vector, hypertrophic maturation and mineralization of chondrocytes were promoted by Cst10 gene overexpression in that type X collagen expression was observed earlier, and alizarin red staining was stronger. On the other hand, type II collagen expression and Alcian blue staining, both of which are markers of the early stage of chondrocyte differentiation, were similar in both cells. Overexpression of the Cst10 gene also caused fragmentation of nuclei, the appearance of annexin V, a change in the mitochondrial membrane potential, and activation of caspases. These results strongly suggest that Cst10 may play an important role in the last steps of the chondrocyte differentiation pathway as an inducer of maturation, followed by apoptosis of chondrocytes.

Endochondral ossification is an essential process for skeletal development, bone growth, and fracture healing and is implicated in pathological conditions such as osteoarthritis and ectopic ossification. During this process, chondrocytes first proliferate and then progressively differentiate into mature hypertrophic chondrocytes. Once fully matured, these hypertrophic cells mineralize the surrounding matrix and undergo apoptosis. This is followed by a local recruitment of blood vessels and osteoclasts, leading to progressive replacement of cartilage by bone. Thus, in this process of endochondral bone formation, proliferation, maturation, mineralization, and apoptosis of chondrocytes must be properly coordinated. To elucidate the molecular mechanisms of endochondral ossification, we have been attempting to isolate novel genes implicated in this process (1–4). For this study, we took advantage of the naturally occurring mouse mutant *ttw* (tiptoe walking), which exhibits ectopic ossification in various soft tissues such as tendons, cartilage, and ligaments of the extremities and the spine (5). We previously found that *ttw* is caused by a nonsense mutation of the nucleotide pyrophosphatase gene encoding an ectoenzyme generating phosphate and pyrophosphate (4). Based on the fact that a high phosphate diet accelerates ectopic ossification of *ttw*, using a differential display method, we identified nine mouse genes whose expression is regulated by a high phosphate diet (1). Six of the nine genes were novel; and among them, we isolated one, termed cystatin 10 (Cst10),[1] that is up-regulated by a high phosphate diet and is expressed exclusively in cartilage, suggesting its specific role in endochondral bone formation.

In this study, we first characterized temporal and spatial expression patterns of Cst10, a novel member of the cystatin superfamily. The cystatin superfamily is known to inhibit the papain-like cysteine proteinases cathepsins B, H, and L by the formation of a tight reversible complex (6). These cysteine proteinases are thought to be associated with terminal degradation of proteins in lysosomes, so the cystatin superfamily is ubiquitously expressed and exhibits various biological functions (7). However, the present study reveals that Cst10 is expressed exclusively in mature chondrocytes. In addition, overexpression of the Cst10 gene accelerates hypertrophic maturation, mineralization, and apoptosis of chondrocytes. These data suggest a crucial and specific role of Cst10 in the later stage of endochondral ossification, implying a physiological role distinct from those other members of the cystatin superfamily.

EXPERIMENTAL PROCEDURES

Determination of the Genomic Structure of the Mouse Cst10 Gene—Bacterial artificial chromosome (BAC) clones containing the mouse Cst10 gene were isolated using a BAC PCR screening system (Genome Systems, St. Louis, MO) according to the manufacturer's protocol. The set of primers used for screening was Cst10/BAC/F (5′-TCCTGAGGATATATGTCAGGC-3′) and Cst10/BAC/R (5′-ATCTCTGTCTGAGGAAAGGAG-3′). To determine the size of introns of the Cst10 gene, interexon PCRs were carried out with primers designed according to the cDNA sequence we determined in this study. The BAC clones and PCR products were sequenced directly, and the exon-intron junctions were

* This work was supported by Grant-in-aid for Scientific Research 14370454 from the Japanese Ministry of Education, Culture, Science, Sports, and Technology and by a grant-in-aid from the Investigation Committee on the Ossification of Spinal Ligaments, Japanese Ministry of Public Health and Welfare. The costs of publication of this article were defrayed in part by the payment of page charges. This article must therefore be hereby marked "*advertisement*" in accordance with 18 U.S.C. Section 1734 solely to indicate this fact.

** To whom correspondence and reprint requests should be addressed: Dept. of Orthopedic Surgery, Faculty of Medicine, University of Tokyo, Hongo 7-3-1, Bunkyo-ku, Tokyo 113-8655, Japan. Tel.: 81-3-5800-8656; Fax: 81-3-3818-4082; E-mail: kawaguchi-ort@h.u-tokyo.ac.jp.

[1] The abbreviations used are: Cst10, cystatin 10; BAC, bacterial artificial chromosome; FITC, fluorescein isothiocyanate; RT, reverse transcription; CstC, cystatin C; PBS, phosphate-buffered saline; PI, propidium iodide; *p*NA, *p*-nitroanilide; BMP, bone morphogenetic protein; PTHrP, parathyroid hormone-related protein.

determined by comparing the genomic sequences obtained with the corresponding cDNA sequences.

Chromosomal Localization—To determine the chromosomal localization of the mouse Cst10 gene, we performed fluorescence *in situ* hybridization as described previously (8). A BAC clone containing the mouse Cst10 gene was labeled and hybridized to the mouse metaphase chromosome. Hybridization signals were rendered visible with fluorescein isothiocyanate (FITC)-avidin. Precise assignments of the signals were determined by visualization of the replicated G-bands.

Animals—The ddY and *ttw* mice were purchased from Shizuoka Laboratories Animal Center (Shizuoka, Japan) and the Central Institute for Experimental Animals (Kanagawa, Japan), respectively. All animal experiments were performed according to the guidelines of the International Association for the Study of Pain (9).

Cell Culture—Primary mesenchymal cells (osteoblasts, chondrocytes, and fibroblasts) were extracted from the calvariae, costal cartilage, and skin, respectively, of neonatal ddY mice as described previously (10, 11). Cells were cultured in α-modified minimal essential medium (Invitrogen) containing 5% fetal bovine serum (Invitrogen) at 37 °C. Mouse chondrogenic ATDC5 cells were obtained from the RIKEN Cell Bank (Saitama, Japan). The cells were cultured in medium consisting of a 1:1 mixture of Dulbecco's modified Eagle's medium and Ham's F-12 medium (Invitrogen) containing 5% fetal bovine serum, 10 μg/ml human transferrin (Roche Applied Science, Mannheim, Germany), and 3×10^{-8} M sodium selenite (Sigma) as described previously (12). The inoculum density of the cells was 4×10^4 cells/well in 12-multiwell plates (Corning Inc., New York). For induction of chondrogenesis, the cells were cultured in medium supplemented with 10 μg/ml bovine insulin (Wako Pure Chemicals, Osaka, Japan). Cells were maintained at 37 °C in a humidified atmosphere of 5% CO_2 in air. The medium was replaced every other day.

Expression of the Cst10 Transcript—Expression of the Cst10 mRNA was examined by semiquantitative reverse transcription (RT)-PCR, followed by Southern blotting using auricular cartilage from *ttw* mice, mesenchymal cells from neonatal ddY mice, and cultured mouse chondrogenic ATDC5 cells. For the experiments with *ttw* mice, the mice were divided into two groups according to the content of phosphate in the diet, *i.e.* high (0.87%) and low (0%) phosphate groups after weaning at 3 weeks of age. The animals were killed 0, 1, 3, 5, 7, 10, and 14 days after the start of the diet, and the auricular cartilage was resected *en bloc*. Total RNAs were extracted using TRIzol reagent (Invitrogen) according to the manufacturer's protocol. RT-PCR was done using the following set of primers: Cst10/3′/F (5′-TCC TGA GGA TAT ATG TCA AT-3′) and Cst10/3′/R (5′-GAA CAG TGG GCC TTT GAA AA-3′). The following amplification cycle was used: 2 min of initial denaturation at 94 °C, followed by 35 cycles at 94, 60, and 72 °C for 30 s each plus extension at 72 °C for 4 min. The primers and RT-PCR conditions used for type II and X collagens were as described previously (13). PCR products were electrophoresed and detected by Southern hybridization. For quantification of type X collagen mRNA levels, the density of each band was measured by NIH Image Version 1.62 [2] and is expressed as the ratio to the density of glyceraldehyde-3-phosphate dehydrogenase.

Immunoblot Analysis—Polyclonal antibody against the full-length Cst10 protein was raised in rabbits using a synthetic peptide of Cst10. For preparation of the whole cell lysate, adherent and detached cells were collected and resuspended in chilled lysis buffer (10 mM Tris-HCl (pH 7.4), 1% Nonidet P-40, 0.1% SDS, 1 mM EDTA, 2 mM sodium orthovanadate, 10 mM sodium fluoride, and 10 mg/ml aprotinin). Collected cells were allowed to lyse by sonication on ice. The homogenate was centrifuged for 5 min in a microcentrifuge at 4 °C, and the supernatants were collected and boiled in SDS sample buffer. The culture medium was collected and centrifuged for 5 min in a microcentrifuge at 4 °C, and the supernatants were collected. The pellet obtained from the supernatants by centrifugation at 19,000 × *g* for 20 min was resuspended in SDS sample buffer. Fifty-μg portions of SDS sample buffer were loaded onto SDS-polyacrylamide gels and blotted onto polyvinylidene difluoride membrane (Amersham Biosciences). Mouse recombinant cystatin C (CstC) protein was purchased from Santa Cruz Biotechnology (Santa Cruz, CA). Protein bands on Western blots were visualized by chemiluminescent detection (ECL, Amersham Biosciences).

Immunohistochemistry—The samples harvested from embryonic mice (18 days postcoitus) were demineralized in 10% EDTA for 1 week at 4 °C. The specimens were dehydrated with increasing concentrations of ethanol and then embedded in paraffin. Cst10 immunolocalization was examined in 4-μm-thick dewaxed paraffin sections. The sections were treated with phosphate-buffered saline (PBS) containing 0.3% hydrogen peroxide for 30 min at room temperature and then with PBS containing 1% bovine serum albumin (Sigma) for 60 min at room temperature. They were then incubated with polyclonal antibody against mouse Cst10 for 24 h at 4 °C and with horseradish peroxidase-conjugated goat anti-rabbit IgG antibody (Dakopatts, Glostrup, Denmark) at a dilution of 1:500 for 1 h at room temperature. After washing with PBS, the sections were immersed in diaminobenzidine solution for 10 min at room temperature for visualization and counterstained with hematoxylin. Nonimmune rabbit serum at the same concentration was used as a negative control. For ultrastructural analysis, these sections were observed under a transmission electron microscope (H-7100, Hitachi, Tokyo) following the pre-embedding method described previously (14). Briefly, embryonic mice (18 days postcoitus) were perfused through the left ventricle with a 2-ml dose of a mixture of 4% paraformaldehyde and 0.1% glutaraldehyde in 0.08 M cacodylate buffer (pH 7.4). The tibiae were then removed and immersed in the same fixative for 2 h at 4 °C. Specimens were decalcified with 4.13% EDTA at 4 °C for 1 day and cryosectioned at a thickness of 10 μm by cryomicrotome. The cryosections were treated following methods similar to those used for immunohistochemical investigations, being post-fixed in 1% OsO_4 in 0.1 M cacodylate buffer at 4 °C for 1 h. The specimens were dehydrated in a graded ethanol series and embedded in Poly/Bed 812 resin (Polysciences, Warrington, PA). Ultrathin sections stained with lead citrate were used for transmission electron microscopic observation.

Establishment of ATDC5 Cells Stably Transfected with the Cst10 Gene—The entire sequence of Cst10 cDNA was amplified by PCR using *Pfu* DNA polymerase (Stratagene, La Jolla, CA) and inserted into the mammalian expression vector pcDNA3.1 (Invitrogen) including the cytomegalovirus promoter with a hemagglutinin epitope tag at the C terminus (pCMV-Cst10). The subcloned cDNA fragment was confirmed by sequencing. ATDC5 cells (2×10^5) were plated in a 6-cm culture dish 24 h before transfection. pCMV-Cst10 (4 mg/6-cm culture dish) or the mock vector (pCMV) was transfected into ATDC5 cells by lipofection using SuperFect transfection reagent (QIAGEN GmbH, Hilden, Germany) according to the manufacturer's instructions. Two days later, cells were diluted 10-fold and incubated in a maintenance medium containing 400 μg/ml Geneticin (Invitrogen). After 2 weeks, we isolated drug-resistant colonies, each of which was derived from a single clone, and cultured them separately. To confirm the reproducibility of the effects of Cst10 overexpression, we performed two experiments with independent transfection procedures. For the first experiment, we established 18 stable clones from 18 different colonies of ATDC5 cells transfected with pCMV-Cst10 and selected three clones (clones 3, 8, and 12) with the highest expression of Cst10 (pCMV-Cst10/ATDC5) by RT-PCR analysis. Three mock vector-transfected clones (clones 1–3) that were confirmed by RT-PCR not to express Cst10 were also selected as negative controls (pCMV/ATDC5). For the second experiment, we independently transfected pCMV-Cst10 into ATDC5 cells as described above, randomly established four stable clones, and examined the relationship of expressions between Cst10 and collagens by RT-PCR.

Alcian Blue and Alizarin Red Staining—pCMV-Cst10/ATDC5 and pCMV/ATDC5 cells were placed in 12-multiwell plates and cultured. Twenty-one days after induction by insulin, cells were rinsed with PBS and fixed with 95% methanol for 20 min. They were then stained overnight with 0.1% Alcian blue 8GS (Fluka, Buchs, Switzerland) in 0.1 M HCl. Twenty-eight days after induction by insulin, cultures were stained with 1% alizarin red S (pH 4.0) (Sigma) after fixation with 95% ethanol.

Detection of Apoptosis and Activities of Caspases—Apoptosis of pCMV-Cst10/ATDC5 and pCMV/ATDC5 cells was examined by nuclear staining with Hoechst 33342, externalization of phosphatidylserine residues using FITC-labeled annexin V, mitochondrial membrane potential, and flow cytometric analysis. Annexin V binding assay was performed using an FITC-labeled annexin V apoptosis detection kit (Medical and Biological Laboratories, Nagoya, Japan) according to the manufacturer's protocol (15–17). Briefly, ATDC5 cells were harvested 7 days after induction with insulin and washed with PBS. Cells were then incubated with binding buffer (10 mM HEPES (pH 7.4), 150 mM NaCl, 5 mM KCl, 1 mM $MgCl_2$, and 1.8 mM $CaCl_2$) containing 2 μl of FITC-labeled annexin V and 5 μg of propidium iodide (PI) for 15 min at room temperature in the dark. After incubation, they were viewed under a fluorescent microscope. PI was added to distinguish cells with membrane permeability due to the loss of membrane integrity, which is characteristic of necrotic cell death. To assess the mitochondrial membrane potential, a MitoCapture apoptosis detection kit (Medical and Biological Laboratories) was used (18). ATDC5 cells harvested 7 days

[2] Available at rsb.info.nih.gov/nih-image/download.html.

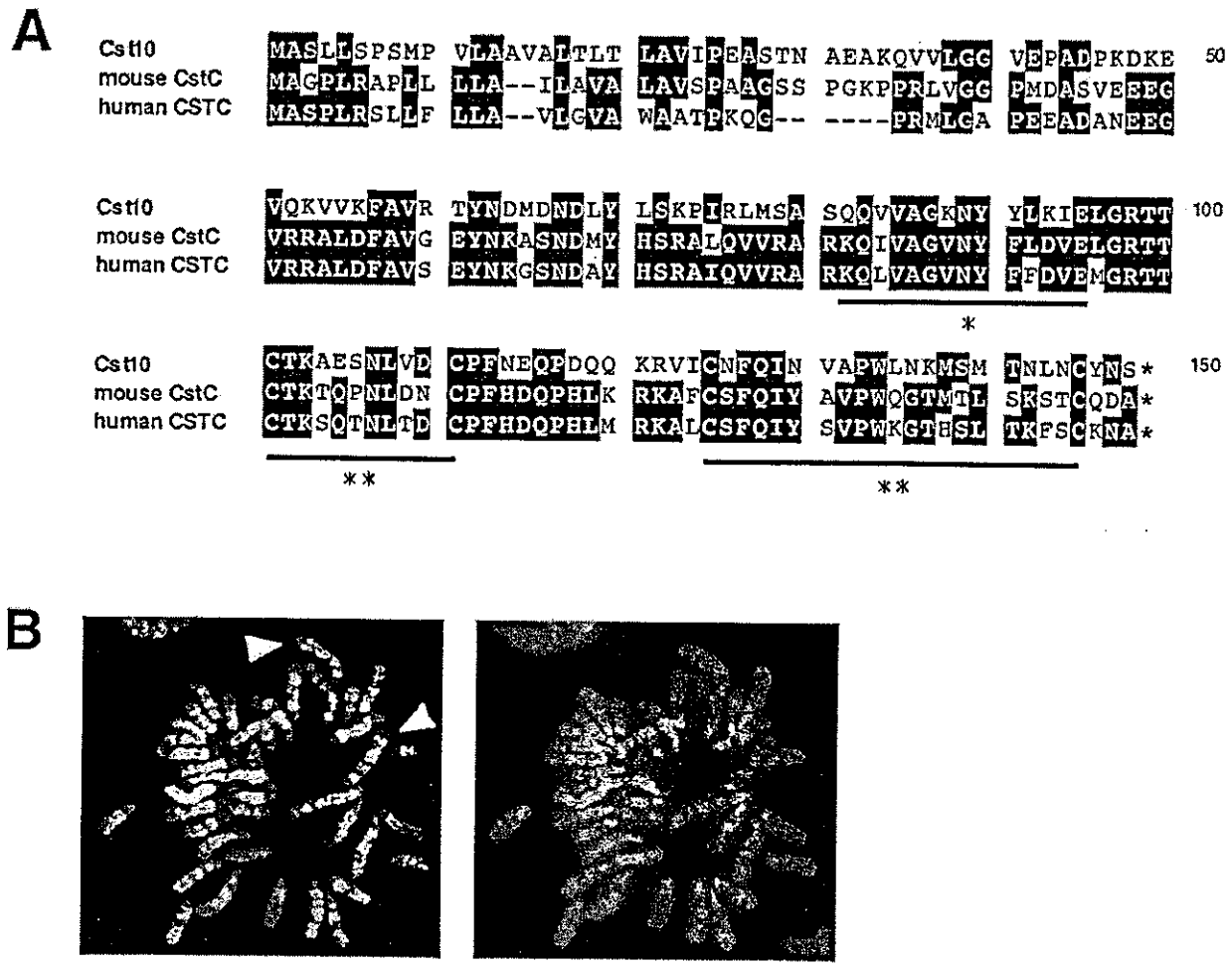

FIG. 1. **Amino acid sequence (*A*) and chromosomal localization (*B*) of the mouse Cst10 gene.** *A*, alignment of the predicted amino acid sequences of the Cst10 gene is shown, and the *highlighted* letters indicate matching bases with the mouse and human CstC genes. The Cst10 gene encodes a protein containing two intrachain disulfide bridges (**) and a cystatin domain (*), indicating a member of the type II cystatin superfamily. *B*, the localization of the Cst10 gene in the mouse chromosome was examined by fluorescence *in situ* hybridization using a BAC clone containing the mouse Cst10 gene as a probe. Hybridization signals were rendered visible with FITC-avidin. Specific hybridization signals were identified at chromosome 2 (*arrowheads*).

after induction were incubated with MitoCapture solution for 15 min at 37 °C and viewed under a fluorescent microscope using a band-pass filter (detects FITC and rhodamine). In healthy cells, MitoCapture accumulates and aggregates in the mitochondria, giving off a bright red fluorescence. In apoptotic cells, MitoCapture cannot aggregate in the mitochondria due to the altered mitochondrial membrane potential and thus remains in the cytoplasm in its monomer form, fluorescing green. For flow cytometric analysis, ATDC5 cells were harvested 0, 1, 3, 5, 7, 10, and 14 days after induction by insulin and fixed with 75% ethanol and PBS at 4 °C for 1 h. After rinsing twice with PBS, cells were incubated for 30 min with 1 ml of PBS containing 1 mg of boiled RNase at 37 °C and then stained with 1 ml of PBS containing 10 μg of PI. A total of 2×10^4 cells were analyzed with a flow cytometer (FACSCaliber, BD Biosciences). To determine whether caspase-3 is activated in pCMV-Cst10/ATDC5, a PhiLux kit (Medical and Biological Laboratories) was used according to the manufacturer's protocol (19). Briefly, ATDC5 cells harvested 7 days after induction were incubated with 10 mM GDEVDGI and labeled with two molecules of rhodamine, which was selectively cut by caspase-3. After incubation, cells were viewed under a fluorescent microscope. Caspase-3 activity was determined with a caspase-3/CPP32 colorimetric protease assay kit (Medical and Biological Laboratories) according to the manufacturer's protocol. In brief, ATDC5 cells were harvested 7 days after induction with insulin and lysed in lysis buffer. Cell lysate (150 μg of protein in 50 μl of lysis buffer) was incubated with DEVD-*p*-nitroanilide (*p*NA) as a substrate for 1 h at 37 °C, and the amount of *p*NA generated was determined spectrophotometrically at 405 nm. Caspase-8 and caspase-9 activities were determined with caspase-8/FLICE and caspase-9/Mch6 colorimetric protease assay kits, respectively (Medical and Biological Laboratories), according to the manufacturer's protocols. IETD-*p*-nitroanilide for caspase-8 and LEHD-*p*-nitroanilide for caspase-9 were used as substrates. After incubation for 1 h at 37 °C, the amount of *p*-nitroanilide generated was determined spectrophotometrically at 405 nm (20–22).

Statistical Analysis—Means of groups were compared by analysis of variance, and significance of differences was determined by post-hoc testing using Bonferroni's method.

RESULTS

Characterization of the Cst10 Gene—In a previous study, using differential display analysis, we identified nine genes, including Cst10, whose expression is regulated in the auricular cartilage of *ttw* mice fed a high phosphate diet (1). The full-length cDNA sequence of the mouse Cst10 gene determined by 5′-rapid amplification of cDNA ends is 789 bp long and has an open reading frame of 447 bp, coding for 148 amino acids (DDBJ/GenBank™/EBI accession number AB036743). The mouse Cst10 gene consists of three exons spanning 4.2 kb on genomic DNA. All of the sequences of the exon-intron junction were confirmed to be the consensus sequences for splicing boundaries (AG/GT rule). The predicted amino acid sequence contains two intrachain disulfide bridges and a cystatin domain (consensus (GSTEQKRV)Q(LIVT)(VAF)(SAGQ)G*X*-(LIVMNK)X_2(LIVMFY)*X*(LIVMFYA)(DENQKRHSIV)), indi-

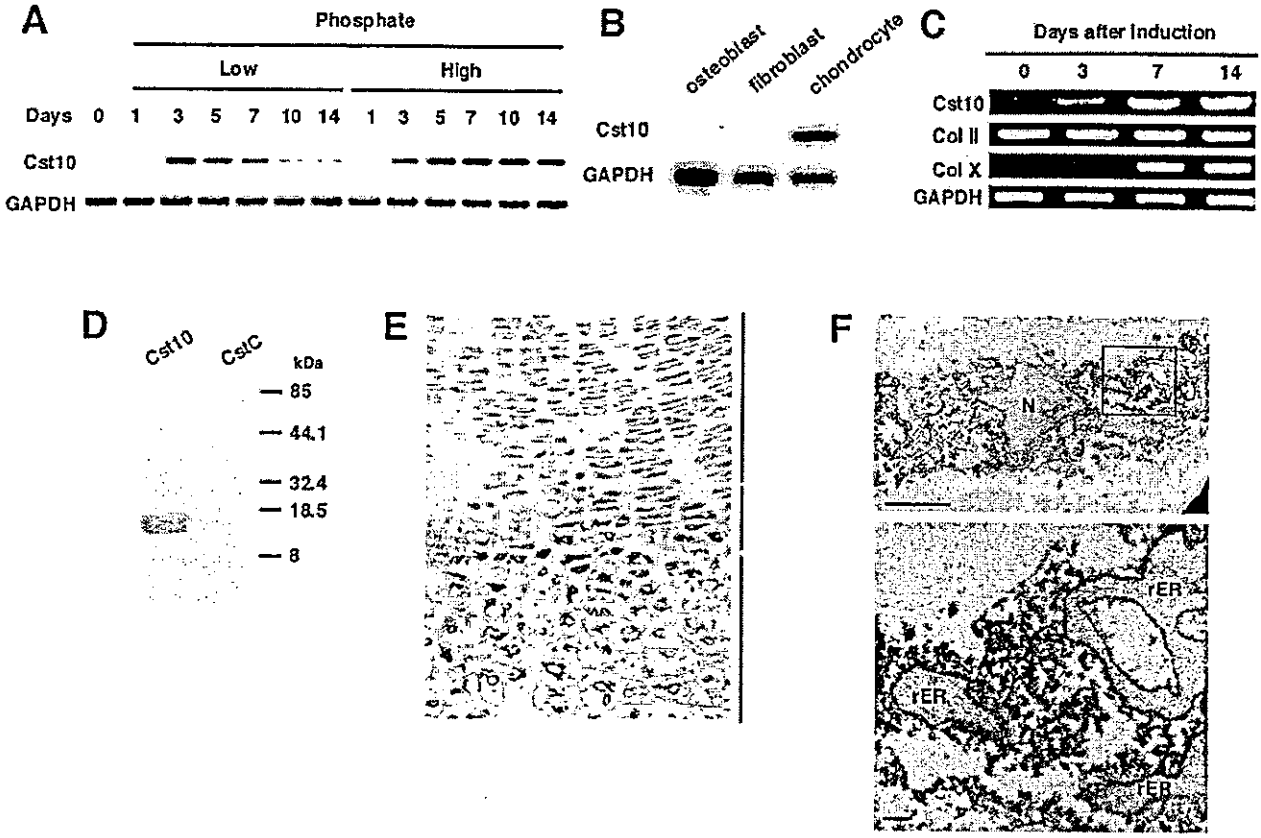

FIG. 2. **Temporal and spatial expression of Cst10.** *A*, time course of Cst10 mRNA expression in the auricular cartilage of *ttw* mice fed high and low phosphate diets. Mice were serially killed at the indicated days after weaning and the start of the diet at 3 weeks of age, and total RNAs were extracted from resected auricular cartilage. Expression was examined by semiquantitative RT-PCR, followed by Southern blotting. *B*, expression of Cst10 mRNA in cultured primary osteoblasts, chondrocytes, and fibroblasts. Cells were isolated from the calvariae, costal cartilage, and skin of neonatal ddY mice, respectively. Expression was examined by semiquantitative RT-PCR, followed by Southern blotting. *C*, temporal expression patterns of Cst10, type II collagen (*Col II*), and type X collagen (*Col X*) during differentiation of mouse chondrogenic ATDC5 cells. At the indicated days after induction with insulin, cells were harvested, and mRNA levels were examined by semiquantitative RT-PCR. *D*, specific reaction of the polyclonal antibody against Cst10 used in this study. The antibody was confirmed to bind to mouse recombinant Cst10, but not to mouse recombinant CstC, by Western blot analysis. *E*, light microscopic immunohistochemistry of Cst10 in the growth plate of an embryonic ddY mouse (18 days postcoitus). *Blue*, *red*, and *green lines* indicate proliferative, prehypertrophic, and hypertrophic layers, respectively. Immunopositive cells are stained *brown*. *F*, electron microscopic immunohistochemistry of Cst10 in a hypertrophic chondrocyte in the growth plate of an embryonic ddY mouse (18 days postcoitus). The *lower panel* shows an enlargement of the *boxed area* in the *upper panel*. Immunochemical localizations shown as electron-dense particles (*asterisks*) were observed in the cytosolic areas, but not in the nucleus (*N*) or the rough endoplasmic reticulum (*rER*). *Bars*, 10 μm (*upper panel*) and 1 μm (*lower panel*). *GAPDH*, glyceraldehyde-3-phosphate dehydrogenase.

cating a novel member of the type II cystatin superfamily with 40.5 and 39.0% homologies to mouse and human CstC (Cst3), respectively, the closest cystatin family member (Fig. 1*A*). Its homologies to other mouse cystatins were around or less than 30%: 31.5% to Cst9, 31.4% to Cst7, 27.0% to CstEM, 28.6% to CstSC, and 26.7% to CstTE. To investigate the localization of the Cst10 gene in the mouse chromosome, >50 metaphase cells were examined by fluorescence *in situ* hybridization using a BAC clone containing the mouse Cst10 gene as a probe. Specific hybridization signals were identified on chromosome 2 in almost all cells, and no significant background was observed at any other chromosomal sites (Fig. 1*B*).

Temporal and Spatial Expression of Cst10 in Vivo and in Vitro—We first examined the temporal expression pattern of Cst10 mRNA levels in the auricular cartilage of *ttw* mice whose endochondral ossification was enhanced with a high phosphate diet. Expression appeared 3 days after weaning and was upregulated by a high phosphate diet at 5 days and thereafter (Fig. 2*A*). Our previous study on the tissue distribution of Cst10 expression in a variety of mouse tissues showed that this gene is expressed exclusively in cartilage (1). We therefore examined the expression pattern of Cst10 using cell cultures. Among three cultured mesenchymal cells from neonatal ddY mice (primary osteoblasts from calvariae, chondrocytes from costal cartilage, and fibroblasts from skin), Cst10 expression was confirmed to be specific to chondrocytes (Fig. 2*B*). To characterize the expression pattern during differentiation of chondrocytes, we used the mouse chondrogenic cell line ATDC5, which can be induced to differentiate into mature chondrocytes in the presence of insulin (12). During induction of differentiation with insulin, expression of type II collagen remained unchanged throughout the culture period up to 14 days, whereas that of type X collagen, a marker for hypertrophic chondrocytes, appeared 7 days after induction (Fig. 2*C*). Expression of the Cst10 gene appeared at 3 days and increased thereafter, indicating that Cst10 expression is in synchrony with the maturation of chondrocytes.

To examine the localization of Cst10 in cartilage, we first confirmed by Western blot analysis the specificity of a polyclonal antibody against Cst10 without cross-reactivity with CstC, the closest member of the cystatin superfamily (Fig. 2*D*). Using this antibody, we performed immunohistochemical analysis on the growth plates of embryonic ddY mice and found that Cst10 was expressed mainly in mature chondrocytes, including

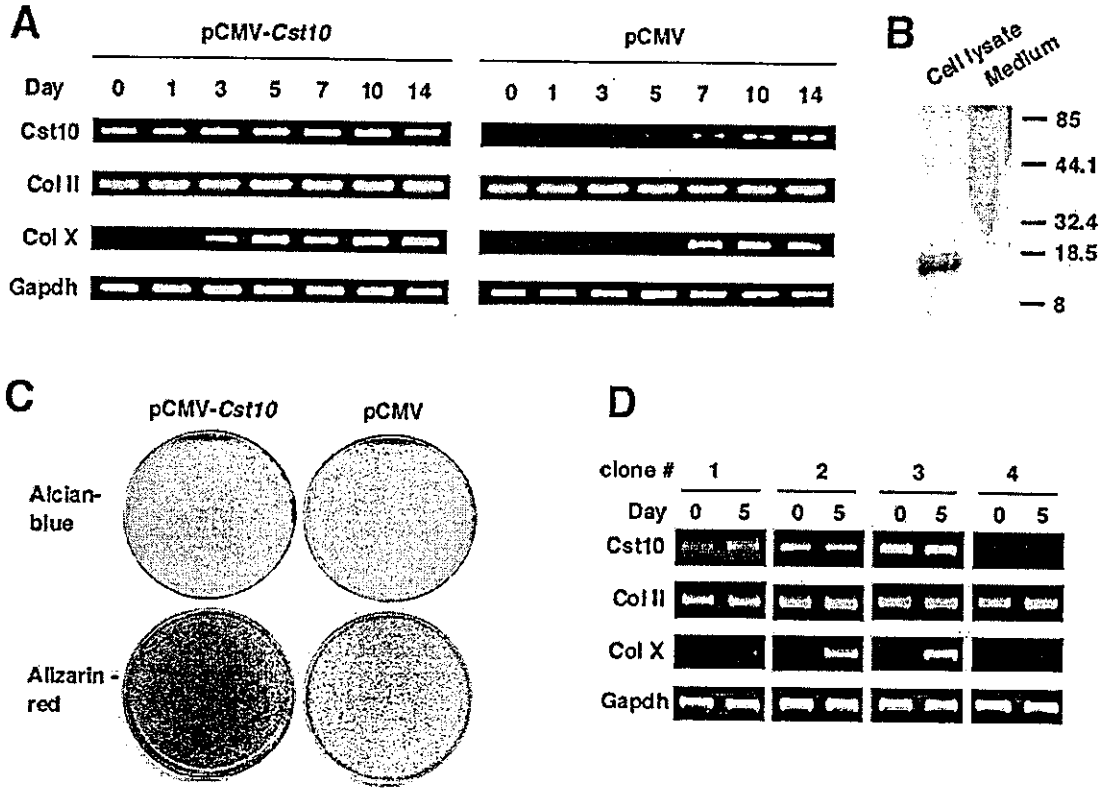

FIG. 3. **Effect of Cst10 overexpression on maturation of ATDC5 cells.** We performed two experiments with independent transfection of the Cst10 gene. For the first experiment (*A–C*), 18 stable clones of ATDC5 cells transfected with pCMV-Cst10 were established as described under "Experimental Procedures," and three clones (clones 3, 8, 12) with the highest expression of Cst10 (pCMV-Cst10/ATDC5) were selected by RT-PCR analysis. Three clones (clones 1–3) transfected with the mock vector (pCMV/ATDC5) were also selected as negative controls. Although the data shown in *A–C* are for representative clones (clone 3 for pCMV-Cst10/ATDC5 and clone 1 for pCMV/ATDC5), the results were reproducible when other clones in each group (clones 8 and 12 for pCMV-Cst10/ATDC5 and clones 2 and 3 for pCMV/ATDC5) were used. *A*, shown are the temporal expression patterns of Cst10, type II collagen (*Col II*), and type X collagen (*Col X*) during differentiation of pCMV-Cst10/ATDC5 and pCMV/ATDC5 cells cultured in the presence of insulin. At the indicated days after induction with insulin, cells were harvested, and the mRNA levels were examined by semiquantitative RT-PCR. *B*, Cst10 protein levels in the cell lysate and medium of pCMV-Cst10/ATDC5 cells cultured for 5 days in the presence of insulin were determined by Western blot analysis. The Cst10 protein could not be detected in the culture medium even if it was lyophilized and condensed (data not shown). *C*, pCMV-Cst10/ATDC5 and pCMV/ATDC5 cells were stained with Alcian blue and alizarin red at 21 and 28 days of culture, respectively, in the presence of insulin. *D*, for the second experiment, ATDC5 cells were transfected with pCMV-Cst10, independent of the first experiment, and four stable clones (clones 1–4) were randomly established. Expression of Cst10 and type II and X collagens was compared among the clones by semiquantitative RT-PCR before (time 0) and 5 days after induction with insulin. *Gapdh*, glyceraldehyde-3-phosphate dehydrogenase.

prehypertrophic and hypertrophic cells (Fig. 2*E*). Electron microscopic examination of a hypertrophic chondrocyte revealed that Cst10 was immunolocalized in the cytosolic areas, but was not found in the nucleus or within the lumen of the rough endoplasmic reticulum (Fig. 2*F*). These findings suggest that Cst10 is not transported into the Golgi-endoplasmic reticulum system, but acts as an intracellular protein in the cytosol.

Overexpression of the Cst10 Gene Accelerates Maturation of ATDC5 Cells—To elucidate the function of Cst10 in chondrocytes, we established stable clones of ATDC5 cells overexpressing the Cst10 gene (pCMV-Cst10/ATDC5). We first compared by RT-PCR the differentiation of pCMV-Cst10/ATDC5 cells with that of control clones of ATDC5 cells transfected with the mock vector (pCMV/ATDC5) upon induction with insulin (Fig. 3*A*). In pCMV-Cst10/ATDC5 cells, Cst10 mRNA expression was clearly seen not only after, but also before induction (time 0), whereas in pCMV/ATDC5 cells, expression was faintly seen 7 days after induction and increased moderately thereafter. Western blot analysis revealed that the Cst10 protein was localized in the cell lysate, but not in the culture medium of pCMV-Cst10/ATDC5 cells (Fig. 3*B*), indicating that Cst10 is not a secreted protein. Expression of type II collagen, which is known to be produced by chondrocytes from their early phase of differentiation, was constitutively seen before and after induction, and expression was not different between pCMV-Cst10/ATDC5 and pCMV/ATDC5 cells (Fig. 3*A*). However, expression of type X collagen, a marker of hypertrophic chondrocytes, was observed earlier and was stronger in pCMV-Cst10/ATDC5 cells than in pCMV/ATDC5 cells. We also compared the cartilage nodule formation and mineralization between cultured pCMV-Cst10/ATDC5 and pCMV/ATDC5 cells using Alcian blue and alizarin red staining, respectively. No difference was seen in the Alcian blue staining between the two cells; however, alizarin red staining was stronger in cultured pCMV-Cst10/ATDC5 cells than in pCMV/ATDC5 cells (Fig. 3*C*).

To confirm the reproducibility of the effects of Cst10 overexpression, we performed another experiment using ATDC5 cell clones that were independently transfected with pCMV-Cst10 and isolated. In this experiment, we randomly established four stable clones and compared the mRNA levels of Cst10 and type II and X collagens by RT-PCR before (time 0) and 5 days after induction (Fig. 3*D*). The Cst10 mRNA levels were not changed before or after induction in all clones. There was a good correlation between the Cst10 and type X collagen levels at 5 days, although the type II collagen levels were similar among the clones (Fig. 3*D*). These results indicate that overexpression of

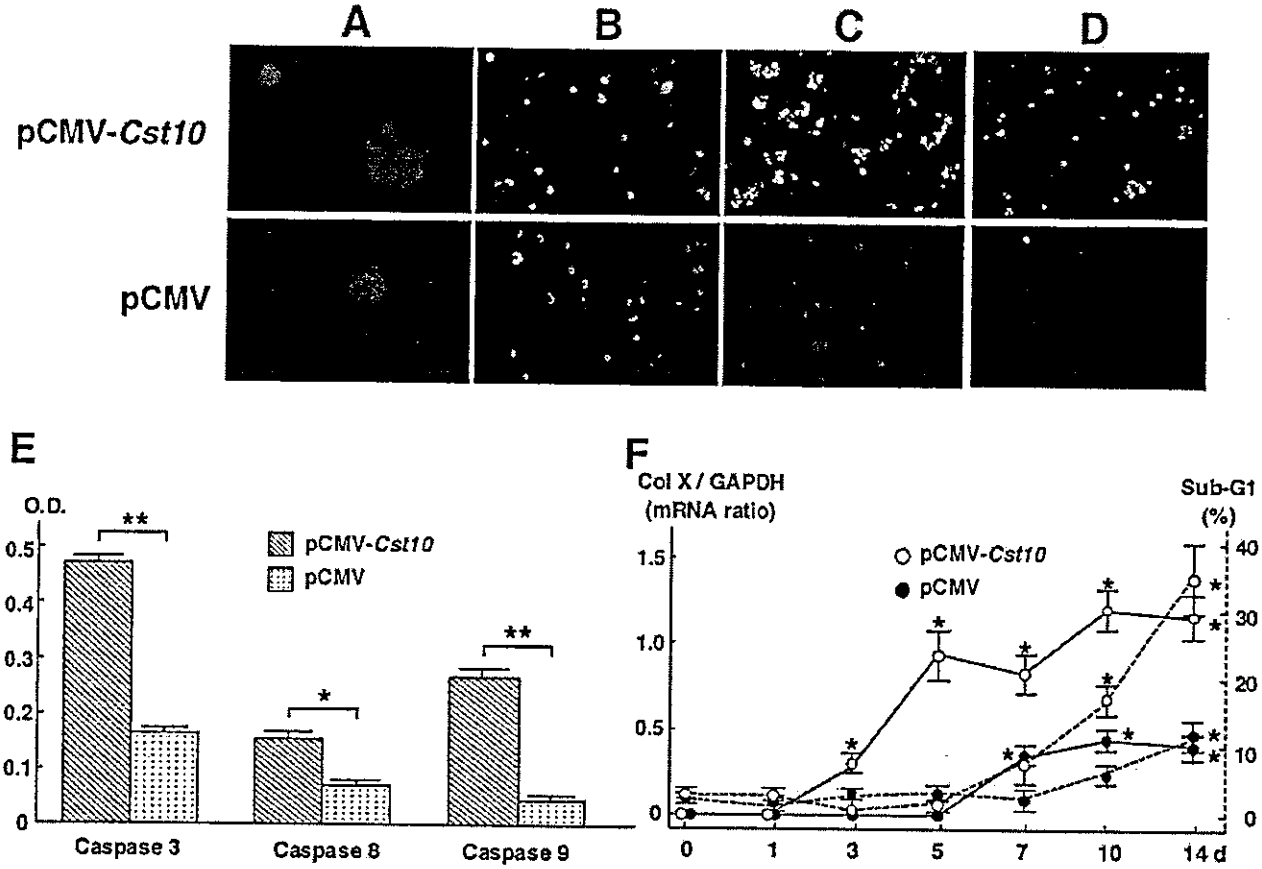

FIG. 4. **Effect of Cst10 overexpression on apoptosis of ATDC5 cells.** *A*, fragmented nuclei immunostained with Hoechst 33342 were seen in pCMV-Cst10/ATDC5 cells. *B*, annexin V-positive cells stained *green* were predominantly seen in pCMV-Cst10/ATDC5 cells, whereas PI-positive cells stained *red* were seen in pCMV/ATDC5 cells. *C*, *green* fluorescence indicating a change in the mitochondrial membrane potential was seen only in pCMV-Cst10/ATDC5 cells, whereas most pCMV/ATDC5 cells gave off *red* fluorescence, indicating healthy mitochondrial membranes. *D*, *green* fluorescence indicating positive caspase-3 activity was predominantly seen in pCMV-Cst10/ATDC5 cells. Although *A–D* are images of representative clones of the first experiment (clone 3 for pCMV-Cst10/ATDC5 and clone 1 for pCMV/ATDC5) 7 days after induction with insulin, similar findings were obtained when two other clones in each group (clones 8 and 12 for pCMV-Cst10/ATDC5 and clones 2 and 3 for pCMV/ATDC5) were used. *E*, shown are the averages of the activities of caspase-3, -8, and -9 in cultured pCMV-Cst10/ATDC5 (clones 3, 8, and 12) and pCMV/ATDC5 (clones 1–3) cells in the first experiment 7 days after induction. The cell lysate was incubated with substrates DEVD-*p*NA, IETD-*p*NA, and LEHD-*p*NA, which were selectively cut by caspase-3, -8, and -9, respectively. The amount of *p*NA free of substrates was measured. Data are expressed as means (*bars*) ± S.E. (*error bars*) for (four cultures/clone) × (three clones/group). *, $p < 0.01$, and **, $p < 0.001$, significant difference between pCMV-Cst10 and pCMV. *F*, shown is the time course of hypertrophic maturation (——) and apoptosis (– – –) of cultured pCMV-Cst10/ATDC5 (○) and pCMV/ATDC5 (●) cells after induction with insulin. Hypertrophic maturation was determined by the ratio of the band densities of type X collagen (*Col X*) and glyceraldehyde-3-phosphate dehydrogenase (*GAPDH*) upon RT-PCR shown in Fig. 3*A*. Apoptosis was determined by the average of the percentage of cells in the sub-G_1 population upon flow cytometric analysis of three clones of each pCMV-Cst10/ATDC5 (clones 3, 8, and 12) and pCMV/ATDC5 (clones 1–3) in the first experiment. Data are expressed as means (*symbols*) ± S.E. (*error bars*) for (four cultures/clone) × (three clones/group). *, $p < 0.01$, significant increase compared with day 0.

the Cst10 gene accelerates the later (but not earlier) stage of chondrocyte differentiation and mineralization.

Overexpression of Cst10 Leads to Apoptosis of ATDC5 Cells—Staining with Hoechst 33342 revealed the existence of cells with fragmented and condensed nuclei with increased fluorescence, suggesting apoptotic cell death in pCMV-Cst10/ATDC5 cells, but not in pCMV/ATDC5 cells (Fig. 4*A*). To distinguish between apoptosis and necrosis in these cells, the kinetics of loss of membrane integrity was examined by double staining with annexin V and PI. Annexin V is known to stain positive in the early stage of apoptotic cells that retain the ability to exclude vital dyes, whereas PI becomes positive in necrotic cells that have lost membrane integrity and that have undergone rapid swelling and lysis (15–17). Most pCMV-Cst10/ATDC5 cells were stained green, indicating that annexin V was positive; however, pCMV/ATDC5 cells were stained red, indicating that PI was positive (Fig. 4*B*). In the analysis of apoptosis through the mitochondrial pathway, many pCMV-Cst10/ATDC5 cells were stained green, indicating the change in the mitochondrial membrane potential, whereas there were no positively stained cells in the pCMV/ATDC5 cell culture (Fig. 4*C*). We further examined the involvement of caspases in the stimulation of chondrocyte apoptosis by Cst10. Staining of substrates specific to caspase-3 revealed that there were many cells with a high activity of this caspase in pCMV-Cst10/ATDC5 cells, but not in pCMV/ATDC5 cells (Fig. 4*D*). Furthermore, we examined the activities of caspase-3, -8, and -9 by measuring *p*NA free of each substrate. pCMV-Cst10/ATDC5 cells exhibited significantly higher activities of all these caspases compared with pCMV/ATDC5 cells (Fig. 4*E*). Caspase-3 and caspase-9, which are known to be associated mainly with the mitochondrial pathway of apoptosis, were strongly activated by Cst10 gene overexpression. These results imply the importance of the mitochondrial pathway in the induction of chondrocyte apoptosis by Cst10.

To determine whether the induction of apoptosis by Cst10 overexpression is a direct action or secondary to that of maturation, we examined the time course of hypertrophic matura-

tion and apoptosis determined by the type X collagen mRNA level shown in Fig. 3*A* and the percentage of cells in the sub-G_1 population by flow cytometric analysis, respectively (Fig. 4*F*). In pCMV-Cst10/ATDC5 cells, significant induction of hypertrophy was seen at 3 days and that of apoptosis at 10 days, whereas in pCMV/ATDC5 cells, hypertrophy was at 7 days and apoptosis at 14 days. Hence, the time gaps between hypertrophy and apoptosis were similar (~7 days) in both cells, suggesting that induction of apoptosis by overexpression of the Cst10 gene may not be direct, but is secondary to that of hypertrophic maturation.

DISCUSSION

Based on our previous study in which we identified a novel gene (Cst10) whose expression is up-regulated during ossification of auricular cartilage by a high phosphate diet in *ttw* mice (1), in the present study, we investigated the possible role of Cst10 in endochondral ossification. Expression was seen exclusively in differentiated chondrocytes in both *in vivo* and *in vitro* mouse models. Overexpression of the Cst10 gene in ATDC5 cells induced their maturation, followed by apoptosis, suggesting an important role of Cst10 in the last steps of chondrocyte differentiation.

Cst10 is a novel member of the cystatin superfamily and shows ~40% homology to both mouse and human CstC. CstC is an abundant extracellular inhibitor of all cysteine proteinases of the papain superfamily (23) and is related to several human disorders such as atherosclerosis and aortic aneurysms (24) and hereditary amyloid angiopathy of the brain (25, 26). CstC also down-regulates bone resorption by inhibiting osteoclastic proteolytic enzymes released into the resorption lacunae in skeletal tissues (27–29). Unlike other members of the cystatin superfamily such as CstC, expression of Cst10 is limited to chondrocytes, implying some specific role of Cst10 in cartilage homeostasis. In addition, electron microscopic examination (Fig. 2*F*) and Western blot analysis (Fig. 3*B*) of cultured pCMV-Cst10/ATDC5 cells indicated that Cst10 is not a secreted protein, but is an intracellular enzyme localized in the cytosol. It is therefore possible that Cst10 has a function distinct from those of other cystatin members that act as extracellular inhibitors of proteinases. Investigation of the physiological role of Cst10 in cartilage *in vivo* is now under way by creating a Cst10 gene-deficient mouse line using homologous recombination in embryonic stem cells.

Regarding the regulation of chondrocyte differentiation and maturation, several secreted molecules have been identified. Bone morphogenetic proteins (BMPs) are reported to be positive regulators, whereas parathyroid hormone-related protein (PTHrP) acts to slow the rate of chondrocyte maturation and to maintain chondrocytes in a proliferative state. Analyses of PTHrP knockout (30, 31) and transgenic (32, 33) mice point to this molecule as a major factor that diminishes the rate of chondrocyte hypertrophy and the subsequent endochondral ossification. Ihh (Indian hedgehog), which co-localizes with BMP-6 in the region of post-proliferative chondrocytes, is known to be another negative regulator of chondrocyte hypertrophy (32, 34). Ihh induces PTHrP expression, and PTHrP reciprocally inhibits Ihh expression, thus forming a negative feedback loop to regulate the rate of chondrocyte hypertrophy. Ihh also blocks BMP-6 expression, suggesting a tightly controlled progression of maturation by secreted molecules within the cartilage (35). Signaling related to cystatins may possibly be involved in the regulatory network of these secreted molecules. In fact, CstC produced by osteoblasts inhibits bone resorption by PTHrP in malignancy (27, 28). In this study as well, ATDC5 cells overexpressing Cst10 showed phenotypes similar to those of chondrocytes from PTHrP-deficient mice: enhanced hypertrophic maturation, mineralization, and apoptosis (30, 31). Studies on the regulation of expression and/or activity of Cst10 by BMPs, PTHrP, and Ihh will help elucidate the molecular mechanism of endochondral ossification in greater detail.

There are many reports demonstrating the association of cysteine proteinases and their inhibitors with apoptotic cell death. Disruption of lysosomal membranes and release of lysosomal enzymes, including proteinases such as cathepsins B (36–38), D (39, 40), and L (41, 42), are known to cause apoptosis (43, 44). This pathway is thought to be mediated mainly by cleavage of the Bcl-2 family member Bid (45). Caspases, which play an integral part in the apoptosis pathway, also belong to a family of cysteine proteinases with aspartate specificity. Some cysteine proteinase inhibitors are reported to block apoptosis (41, 46); and among them, leupeptin and E-64 specifically suppress activation of caspase-3-like proteinases (47). Hence, cystatins could also down-regulate apoptosis by inhibiting lysosomal enzymes or caspases. In fact, loss-of-function mutations in the cystatin B gene cause a severe neurological disorder known as Unverricht-Lundoborg disease in humans (48, 49) and myoclonic seizures and ataxia in mice (50, 51), in which cerebellar granule cells appear to undergo apoptosis. In contrast, CstC has been reported to induce apoptosis in cultured rat neurons (52) and during mouse embryo implantation and placentation (53). The present study has also shown that Cst10 overexpression led to apoptosis in chondrocytes. A direct contribution of proteinases to chondrocyte apoptosis was actually implied by the finding that matrix metalloproteinase-9-deficient mice exhibit normal hypertrophic maturation, but delayed apoptosis (54). However, the action of Cst10 on chondrocyte apoptosis is not likely to be direct, but secondary to its stimulation of maturation, because the time gaps between hypertrophy and apoptosis were similar between cells with and without Cst10 overexpression (Fig. 4*F*). Furthermore, in our preliminary experiments, Cst10 gene overexpression failed to promote apoptosis in the non-chondrogenic cell line COS-7 (data not shown). Recent studies on various knockout mice also suggest that there is a direct coupling between maturation and apoptosis in chondrocytes. PTHrP-deficient mice exhibit acceleration of both hypertrophy and apoptosis in growth plate chondrocytes (30, 31). Mice deficient in Bcl-2, an inhibitor of apoptosis, exhibit premature chondrocyte differentiation (33). Although changes in the mitochondrial membrane potential and related caspases were seen in Cst10-expressing chondrocytes, this also may not be a specific action of Cst10 because normal chondrocyte apoptosis is known to involve Bcl-2, mitochondrial integrity, and caspases (33, 55). Further studies on intracellular interactions between Cst10 and signaling molecules of apoptosis such as Bcl-2 will elucidate more precise mechanisms by which Cst10 overexpression leads to chondrocyte apoptosis.

Chondrocyte maturation, mineralization, and apoptosis in the endochondral ossification process are observed in physiological development and growth as well as under pathological conditions such as osteoarthritis and ectopic ossification. Understanding the molecular mechanisms of endochondral ossification through the Cst10 signaling pathway may therefore help elucidate not only the mechanism of skeletal development and growth, but also the pathophysiology of these diseases.

REFERENCES

1. Koshizuka, Y., Ikegawa, S., Sano, M., Nakamura, K., and Nakamura, Y. (2001) *Cytogenet. Cell Genet.* **94**, 163–168
2. Koshizuka, Y., Ikegawa, S., Sano, M., Nakamura, K., and Nakamura, Y. (2001) *Genomics* **72**, 252–259
3. Ikegawa, S., Sano, M., Koshizuka, Y., and Nakamura, Y. (2000) *Cytogenet. Cell Genet.* **90**, 291–297
4. Okawa, A., Nakamura, I., Goto, S., Moriya, H., Nakamura, Y., and Ikegawa, S. (1998) *Nat. Genet.* **19**, 271–273
5. Hosoda, Y., Yoshimura, Y., and Higaki, A. (1981) *Ryumachi* **21**, 157–164
6. Barrett, A. J., Fritz, H., Grubb, A., Isemura, S., Jarvinen, M., Katunuma, N.,

Machleidt, W., Muller-Esterl, W., Sasaki, M., and Turk, V. (1986) *Biochem. J.* **236**, 312
7. Reinheckel, T., Deussing, J., Roth, W., and Peters, C. (2001) *Biol. Chem. Hoppe-Seyler* **382**, 735–741
8. Inazawa, J., Saito, H., Ariyama, T., Abe, T., and Nakamura, Y. (1993) *Genomics* **17**, 153–162
9. Zimmermann, M. (1983) *Pain* **16**, 109–110
10. Kawaguchi, H., Manabe, N., Miyaura, C., Chikuda, H., Nakamura, K., and Kuro-o, M. (1999) *J. Clin. Investig.* **104**, 229–237
11. Shimoaka, T., Ogasawara, T., Yonamine, A., Chikazu, D., Kawano, H., Nakamura, K., Itoh, N., and Kawaguchi, H. (2002) *J. Biol. Chem.* **277**, 7493–7500
12. Shukunami, C., Ishizeki, K., Atsumi, T., Ohta, Y., Suzuki, F., and Hiraki, Y. (1997) *J. Bone Miner. Res.* **12**, 1174–1188
13. Wang, D., Canaff, L., Davidson, D., Corluka, A., Liu, H., Hendy, G. N., and Henderson, J. E. (2001) *J. Biol. Chem.* **276**, 33995–34005
14. Hoshi, K., Ejiri, S., and Ozawa, H. (2001) *J. Bone Miner. Res.* **16**, 289–298
15. Fadok, V. A., Voelker, D. R., Campbell, P. A., Cohen, J. J., Bratton, D. L., and Henson, P. M. (1992) *J. Immunol.* **148**, 2207–2216
16. Koopman, G., Reutelingsperger, C. P., Kuijten, G. A., Keehnen, R. M., Pals, S. T., and van Oers, M. H. (1994) *Blood* **84**, 1415–1420
17. Martin, S. J., Reutelingsperger, C. P., McGahon, A. J., Rader, J. A., van Schie, R. C., LaFace, D. M., and Green, D. R. (1995) *J. Exp. Med.* **182**, 1545–1556
18. Ogawa, Y., Nishioka, A., Kobayashi, T., Kariya, S., Hamasato, S., Saibara, T., Seguchi, H., and Yoshida, S. (2001) *Int. J. Mol. Med.* **7**, 603–607
19. Komoriya, A., Packard, B. Z., Brown, M. J., Wu, M. L., and Henkart, P. A. (2000) *J. Exp. Med.* **191**, 1819–1828
20. Casciola-Rosen, L., Nicholson, D. W., Chong, T., Rowan, K. R., Thornberry, N. A., Miller, D. K., and Rosen, A. (1996) *J. Exp. Med.* **183**, 1957–1964
21. Datta, R., Kojima, H., Banach, D., Bump, N. J., Talanian, R. V., Alnemri, E. S., Weichselbaum, R. R., Wong, W. W., and Kufe, D. W. (1997) *J. Biol. Chem.* **272**, 1965–1969
22. Thornberry, N. A., Rano, T. A., Peterson, E. P., Rasper, D. M., Timkey, T., Garcia-Calvo, M., Houtzager, V. M., Nordstrom, P. A., Roy, S., Villancourt, J. P., Chapman, K. T., and Nicholson, D. W. (1997) *J. Biol. Chem.* **272**, 17907–17911
23. Abrahamson, M. (1988) *Scand. J. Clin. Lab. Investig.* **48**, 21–31
24. Shi, G. P., Sukhova, G. K., Grubb, A., Ducharme, A., Rhode, L. H., Lee, R. T., Ridker, P. M., Libby, P., and Chapman, H. A. (1999) *J. Clin. Investig.* **104**, 1191–1197
25. Palsdottir, A., Abrahamson, M., Thorsteinsson, L., Arnason, A., Olafsson, I., Grubb, A., and Jensson, O. (1988) *Lancet* **8611**, 603–604
26. Abrahamson, M., Jonsdottir, S., Olafsson, I., Jensson, O., and Grubb, A. (1992) *Hum. Genet.* **89**, 377–380
27. Lerner, U. H., Johansson, L., Ranjso, M., Rosenquist, J. B., Reinholt, F. P., and Grubb, A. (1997) *Acta Physiol. Scand.* **161**, 81–92
28. Lerner, U. H., and Grubb, A. (1992) *J. Bone Miner. Res.* **7**, 433–440
29. Johansson, L., Grubb, A., Abrahamson, M., Kasprzykowski, F., Kasprzykowski, R., Grzonka, Z., and Lerner, U. H. (2000) *Bone (N. Y)* **26**, 451–459
30. Karaplis, A. C., Luz, A., Glowacki, J., Bronson, R. T., Tybulewicz, V. L., Kronenberg, H. M., and Mulligan, R. C. (1994) *Genes Dev.* **8**, 277–289
31. Amizuka, N., Warshawsky, H., Henderson, J. E., Goltzman, D., and Karaplis, A. C. (1994) *J. Cell Biol.* **126**, 1611–1623
32. Vortkamp, A., Lee, K., Lanske, B., Segre, G. V., Kronenberg, H. M., and Tabin, C. J. (1996) *Science* **273**, 613–622
33. Amling, M., Neff, L., Tanaka, S., Inoue, D., Kuida, K., Weir, E., Philbrick, W. M., Broadus, A. E., and Baron, R. (1997) *J. Cell Biol.* **136**, 205–213
34. Bitgood, M. J., and McMahon, A. P. (1995) *Dev. Biol.* **172**, 126–138
35. Grimsrud, C. D., Romano, P. R., D'Souza, M., Puzas, J. E., Reynolds, P. R., Rosier, R. N., and O'Keefe, R. J. (1999) *J. Bone Miner. Res.* **14**, 475–482
36. Isahara, K., Ohsawa, Y., Kanamori, S., Shibata, M., Waguri, S., Sato, N., Gotow, T., Watanabe, T., Momoi, T., Urase, K., Kominami, E., and Uchiyama, Y. (1999) *Neuroscience* **91**, 233–249
37. Foghsgaard, L., Wissing, D., Mauch, D., Lademann, U., Bastholm, L., Boes, M., Elling, F., Leist, M., and Jaattela, M. (2001) *J. Cell Biol.* **153**, 999–1010
38. Guicciardi, M. E., Deussing, J., Miyoshi, H., Bronk, S. F., Svingen, P. A., Peters, C., Kaufmann, S. H., and Gores, G. J. (2000) *J. Clin. Investig.* **106**, 1127–1137
39. Roberg, K. (2001) *Lab. Investig.* **81**, 149–158
40. Zang, Y., Beard, R. L., Chandraratna, R. A., and Kang, J. X. (2001) *Cell Death Differ.* **8**, 477–485
41. Sarin, A., Adams, D. H., and Henkart, P. A. (1993) *J. Exp. Med.* **178**, 1693–1700
42. Katunuma, N., Matsui, A., Kakegawa, T., Murata, E., Asao, T., and Ohba, Y. (1999) *Adv. Enzyme Regul.* **39**, 247–260
43. Fossel, E. T., Zanella, C. L., Fletcher, J. G., and Hui, K. K. (1994) *Cancer Res.* **54**, 1240–1248
44. Brunk, U. T., Dalen, H., Roberg, K., and Hellquist, H. B. (1997) *Free Radic. Biol. Med.* **23**, 616–626
45. Stoka, V., Turk, B., Schendel, S. L., Kim, T. H., Cirman, T., Snipas, S. J., Ellerby, L. M., Bredesen, D., Freeze, H., Abrahamson, M., Bromme, D., Krajewski, S., Reed, J. C., Yin, X. M., Turk, V., and Salvesen, G. S. (2001) *J. Biol. Chem.* **276**, 3149–3157
46. Sarin, A., Clerici, M., Blatt, S. P., Hendrix, C. W., Shearer, G. M., and Henkart, P. A. (1994) *J. Immunol.* **153**, 862–872
47. Ishisaka, R., Utsumi, T., Yabuki, M., Kanno, T., Furuno, T., Inoue, M., and Utsumi, K. (1998) *FEBS Lett.* **435**, 233–236
48. Pennacchio, L. A., Lehesjoki, A. E., Stone, N. E., Willour, V. L., Virtaneva, K., Miao, J., D'Amato, E., Ramirez, L., Faham, M., Koskiniemi, M., Warrington, J. A., Norio, R., de la Chapelle, A., Cox, D. R., and Myers, R. M. (1996) *Science* **271**, 1731–1734
49. Lalioti, M. D., Scott, H. S., Buresi, C., Rossier, C., Bottani, A., Morris, M. A., Malafosse, A., and Antonarakis, S. E. (1997) *Nature* **386**, 847–851
50. Pennacchio, L. A., Bouley, D. M., Higgins, K. M., Scott, M. P., Noebels, J. L., and Myers, R. M. (1998) *Nat. Genet.* **20**, 251–258
51. Lieuallen, K., Pennacchio, L. A., Park, M., Myers, R. M., and Lennon, G. G. (2001) *Hum. Mol. Genet.* **10**, 1867–1871
52. Nishio, C., Yoshida, K., Nishiyama, K., Hatanaka, H., and Yamada, M. (2000) *Brain Res.* **873**, 252–262
53. Afonso, S., Romagnano, L., and Babiarz, B. (1997) *Development* **124**, 3415–3425
54. Vu, T. H., Shipley, J. M., Bergers, G., Berger, J. E., Helms, J. A., Hanahan, D., Shapiro, S. D., Senior, R. M., and Werb, Z. (1998) *Cell* **93**, 411–422
55. Chrysis, D., Ritzen, E. M., and Savendahl, L. (2003) *J. Endocrinol.* **176**, 331–337

The EMBO Journal Vol. 22 No. 24 pp. 6653–6664, 2003

Regulation of osteoclast apoptosis by ubiquitylation of proapoptotic BH3-only Bcl-2 family member Bim

Toru Akiyama, Phillippe Bouillet[1], Tsuyoshi Miyazaki, Yuho Kadono, Hirotaka Chikuda, Ung-il Chung, Akira Fukuda, Atsuhiko Hikita, Hiroaki Seto[2], Takashi Okada[3], Toshiya Inaba[4], Archana Sanjay[5], Roland Baron[5], Hiroshi Kawaguchi, Hiromi Oda, Kozo Nakamura, Andreas Strasser[1] and Sakae Tanaka[6]

Department of Orthopaedic Surgery, Faculty of Medicine, The University of Tokyo, 7-3-1 Hongo, Bunkyo-ku, Tokyo 113-0033, [2]Department of Orthopaedics, Juntendo University, School of Medicine, [3]Division of Genetic Therapeutics, Center for Molecular Medicine, Jichi Medical School, 3311-1 Yakushiji, Minamikawachi, Kawachi, Tochigi 329-0498, [4]Department of Molecular Oncology, Research Institute for Radiation Biology and Medicine, Hiroshima University, Hiroshima 734-8553, Japan, [1]The Walter and Eliza Hall Institute of Medical Research, 1G Royal Parade, Parkville, 3050 Victoria, Australia and [5]Departments of Cell Biology and Orthopaedics, Yale University School of Medicine, New Haven, CT, USA

[6]Corresponding author
e-mail: TANAKAS-ORT@h.u-tokyo.ac.jp

Osteoclasts (OCs) undergo rapid apoptosis without trophic factors, such as macrophage colony-stimulating factor (M-CSF). Their apoptosis was associated with a rapid and sustained increase in the pro-apoptotic BH3-only Bcl-2 family member Bim. This was caused by the reduced ubiquitylation and proteasomal degradation of Bim that is mediated by c-Cbl. Although the number of OCs was increased in the skeletal tissues of *bim*–/– mice, the mice exhibited mild osteosclerosis due to reduced bone resorption. OCs differentiated from bone marrow cells of *bim*–/– animals showed a marked prolongation of survival in the absence of M-CSF, compared with *bim*+/+ OCs, but the bone-resorbing activity of *bim*–/– OCs was significantly reduced. Overexpression of a degradation-resistant lysine-free Bim mutant in *bim*–/– cells abrogated the anti-apoptotic effect of M-CSF, while wild-type Bim did not. These results demonstrate that ubiquitylation-dependent regulation of Bim levels is critical for controlling apoptosis and activation of OCs.

Keywords: apoptosis/bim/M-CSF/osteoclast/ubiquitylation

Introduction

Apoptosis is a genetically programmed process for killing unwanted cells (Kerr *et al.*, 1972). Abnormalities in apoptosis regulation can promote cancer, autoimmune disease or degenerative disorders (Thompson, 1995). Mammals have two distinct apoptosis signaling pathways that converge upon activation of aspartate-specific cysteine proteases (caspases), which mediate cell demolition (Strasser *et al.*, 1995). One pathway is initiated by death receptors, members of the tumor necrosis factor receptor (TNF-R) family with an intracellular death domain, and propagated through FADD adaptor protein-mediated activation of caspase-8. The other pathway is regulated by pro- and anti-apoptotic Bcl-2 family members and involves mitochondrial release of cytochrome c, which causes Apaf-1 adaptor-mediated activation of caspase-9 (Gross *et al.*, 1999; Strasser *et al.*, 2000). The anti-apoptotic Bcl-2 family members include mammalian Bcl-2, Bcl-xL, Bcl-w, Mcl-1, A1 and Boo/Diva, and *Caenorhabditis elegans* CED-9, and they share similarity within three or four Bcl-2 homology (BH) domains. So far, >20 pro-apoptotic Bcl-2 family proteins have been identified in mammals. They can be divided further into two groups: multidomain members possess homology in two or three BH regions (mammalian Bax, Bak, Bok/Mtd, Bcl-xS and Bfk), whereas the BH3 domain-only proteins (mammalian Bik/Nbk, Bad, Bid, Hrk/DP5, Bim/Bod, Noxa, Bmf and Puma/Bbc3, and *C.elegans* EGL-1) share only the short BH3 region (Huang and Strasser, 2000). Genetic studies and experiments with transfected cells have shown that BH3-only proteins are essential for initiation of apoptosis (Huang and Strasser, 2000), whereas Bax/Bak-like proteins play an essential role further downstream (Cheng *et al.*, 2001; Zong *et al.*, 2001). Bax/Bak-like proteins are ubiquitously expressed, whereas BH3-only family members have a more tissue-specific distribution, indicating that the latter may play a tissue/cell-specific and death stimulus-specific role in apoptosis. The pro-apoptotic activity of BH3-only proteins is strictly regulated at both the transcriptional and post-translational level to prevent inappropriate cell killing (Huang and Strasser, 2000).

The BH3-only protein Bim was first identified as a Bcl-2-interacting protein by screening a λ phage expression library constructed from a mouse thymic lymphoma (O'Connor *et al.*, 1998). Bim is expressed in hematopoietic, epithelial, neuronal and germ cells (O'Reilly *et al.*, 2000), and alternative splicing generates various Bim isoforms, including Bim_S, Bim_L and Bim_{EL}. Experiments with knock-out mice have shown that Bim is essential for apoptosis of T lymphocytes, B lymphocytes, myeloid cells and neurons (Bouillet *et al.*, 1999, 2002; Putcha *et al.*, 2001; Whitfield *et al.*, 2001; Villunger *et al.*, 2003). Pro-apoptotic activity of Bim is regulated both transcriptionally and post-transcriptionally (Huang and Strasser, 2000). Osteoclasts (OCs) are multinucleated giant cells primarily responsible for bone resorption (Baron, 1989; Suda *et al.*, 1992; Tanaka *et al.*, 2003). They are terminally differentiated cells, and undergo rapid apoptosis in the absence of

trophic factors such as macrophage colony-stimulating factor (M-CSF) and receptor activator of NF-κB ligand (RANKL) (Hughes *et al.*, 1995). We demonstrate here that Bim is critical for normal OC survival and function.

Results

Rapid induction of Bim protein in cytokine-deprived OCs

To obtain murine OCs, we used a co-culture system of osteoblastic cells and bone marrow cells in the presence of 1α, 25-dihydroxyvitamin D_3 [1α, 25$(OH)_2D_3$] and prostaglandin E_2 (PGE_2), as previously reported (Takahashi *et al.*, 1988). OCs purified from co-cultures by removing osteoblastic cells by collagenase and dispase treatment were then maintained in the presence of M-CSF (10 ng/ml) for an additional 12 h. When M-CSF was removed from the culture, OCs underwent rapid cell death. Within 24 h, 70% of OCs had died and virtually all cells died out after 48 h, as previously reported (Miyazaki *et al.*, 2000). We examined whether cytokine withdrawal caused changes in the expression levels of pro- or anti-apoptotic Bcl-2 family members. Immunoblot analysis revealed a marked increase in Bim expression levels within 3 h of M-CSF removal and it remained high for at least 12 h (Figure 1A), while expression levels of Bid, Bax or Bcl-xL were not affected. Induction of Bim was reversed by M-CSF or, albeit less efficiently, by RANKL treatment for 12 h (Figure 1A). A rapid increase in Bim levels was also observed in cytokine-deprived OC precursors (data not shown). However, no significant difference in *bim* mRNA level was observed between OCs cultured in the presence or absence of M-CSF either by RT–PCR or by real-time PCR (Figure 1C), demonstrating that the changes in Bim protein levels are due to post-tranlational mechanisms.

We previously reported that the Ras/extracellular signal-regulated kinase (ERK) pathway promotes survival of OCs (Miyazaki *et al.*, 2000), while others found that the phosphatidylinositol 3-kinase (PI3-kinase)/Akt pathway has an effect on this process (Wong *et al.*, 1999; Glantschnig *et al.*, 2003). To analyze whether these pathways are involved in downregulation of Bim by M-CSF, we employed adenovirus vectors encoding constitutively active MEK1 (MEK^{CA}) or Akt (myr-Akt), which contains a Src myristoylation signal that promotes association with the plasma membrane, causing constitutive activation. As shown in Figure 1B, enforced expression of MEK^{CA} reversed the induction of Bim after M-CSF removal, while myr-Akt had less effect. Treating the cells with a specific inhibitor of MEK/ERK pathways, PD98059, completely abolished the effect of M-CSF on Bim expression (Figure 1B). These results indicate that Ras/ERK signaling is a major pathway for downregulation of Bim by M-CSF in OCs.

We next examined the effects of Bim and Bcl-xL overexpression in OC apoptosis caused by cytokine withdrawal using adenovirus vectors. Less than 5% of OCs overexpressing Bim survived 12 h after M-CSF removal, whereas 20% of control virus-infected cells remained alive at this time (Figure 1D). Co-expression of Bcl-xL abrogated the pro-apoptotic effects of the Bim_L adenovirus, indicating that the balance between Bim and Bcl-xL may determine the fate of OCs (Figure 1D).

Expression of Bim in skeletal tissues

To determine the expression of *bim* in skeletal tissues, we performed *in situ* hybridization analysis using a bim_L antisense probe which detects bim_S, bim_L and bim_{EL}. Strong expression of *bim* mRNA was observed in the bone trabeculae of 5-week-old male mouse metatarsal bone, which was co-localized with tartrate-resistant acid phosphatase (TRAP) enzymatic staining, i.e. with OCs (Figure 2A and B). On the other hand, *bim* transcripts were hardly detectable in osteoblasts or chondrocytes, whose localization was determined by procollagen type IA and type IIA expression, respectively (Figure 2B–D). The expression pattern of *bim* in the skeletal tissues was confirmed further by X-gal staining of mutant mice, in which a *lacZ* reporter gene was knocked into the *bim* locus by homologous recombination (Figure 2E).

Mild osteosclerosis in Bim-deficient mice is due to reduced bone turnover

We next studied the skeletal tissues of *bim–/–* mice. Histological examination and X-ray analysis revealed that *bim–/–* mice have mild osteosclerosis (Figure 3A). Histomorphometry demonstrated that *bim–/–* mice had abnormally low levels of new bone formation and turnover of the skeletal tissues (Figure 3D and E). The osteoid surface (OS/BS) and osteoblast surface (Ob.S/BS) were lower in *bim–/–* mice compared with wild-type animals (Figure 3D), and calcein double labeling revealed a marked decrease in the mineral apposition rate (MAR) in the *bim–/–* mice (Figure 3E). Although the OC number per bone perimeter (Oc.N/B.Pm) was increased in *bim–/–* mice, the percentage of the eroded surface (ES/BS) and OC surface (Oc.S/BS) was reduced (Figure 3D). It appears likely that this defect is a consequence of the abnormally small size and impaired actin ring formation of the *bim–/–* OCs (Figure 3B and C).

Elongated life span of bim–/– OCs in vivo

We next examined whether *bim–/–* OCs have a longer life span *in vivo* (Figure 3F). Five-week-old *bim+/+* and *bim–/–* mice were fed with water containing 1 mg/ml of 5′-bromo-2′-deoxyuridine (BrdU) for 1 week (labeling period). Mice were then sacrificed either on the next day (group A) or after 6 weeks (group B) of the labeling period. Immunostaining with anti-BrdU antibody demonstrated that almost similar proportions of OCs were positively stained in group A *bim+/+* and *bim–/–* mice (50 and 48%, respectively). However, the proportion of BrdU-positive OCs was markedly decreased to <5% in group B *bim+/+* mice, while that in group B *bim–/–* mice was maintained at 33%. This suggests that *bim–/–* OCs have a longer life span than *bim+/+* OCs *in vivo*.

bim–/– OCs are resistant to cytokine withdrawal-induced apoptosis but have abnormally low bone resorption activity in vitro

Bone marrow cells obtained from *bim–/–* and *bim+/+* mice were subjected to OC formation assay by co-culturing with osteoblastic cells in the presence of 1α,25$(OH)_2D_3$ and PGE_2. The number of TRAP-positive multinucleated cells formed from *bim–/–* bone marrow cells was comparable with that from *bim+/+* cells. The *bim–/–* OCs were,

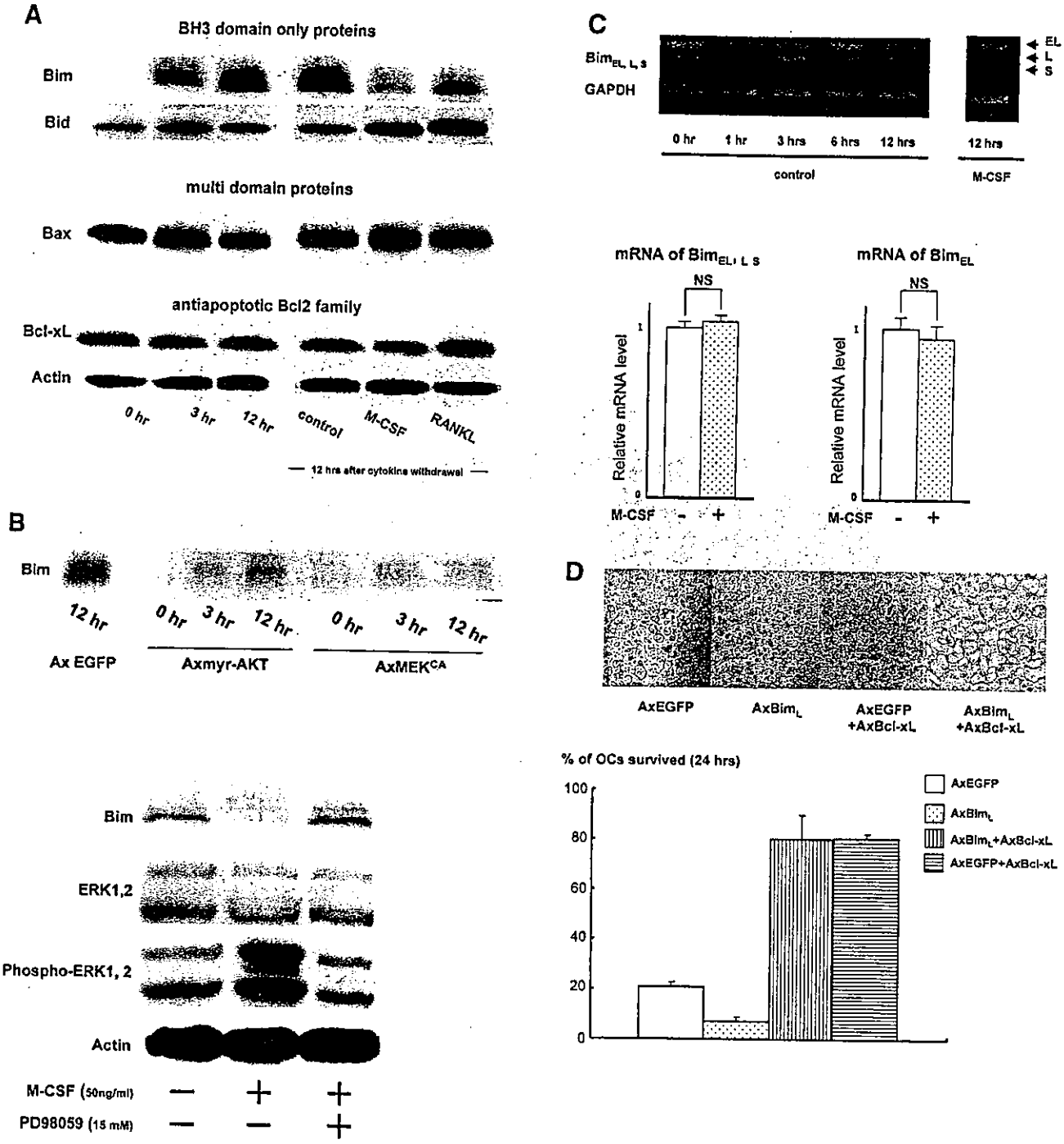

Fig. 1. Regulation of Bim expression in OCs. (A) Cytokine withdrawal caused rapid upregulation of Bim levels in OCs. OCs purified from co-cultures by removing osteoblastic cells by collagenase and dispase treatment were then maintained in the presence of M-CSF (10 ng/ml) for an additional 12 h. The expression levels of Bim and other apoptosis-regulatory proteins in OCs after M-CSF removal were analyzed by western blotting using specific antibodies. Bim levels increased within 3 h, and the upregulation was sustained at least for 12 h. This upregulation of Bim level was strongly suppressed by M-CSF, and to a lesser extent by sRANKL treatment for 12 h. (B) Intracellular signaling pathways leading to Bim downregulation. Upper panel: introduction of MEK^{CA} strongly suppressed the upregulation of Bim after M-CSF removal. Overexpression of myr-Akt had less effect on Bim expression in OCs. Lower panel: treating the cells with a specific inhibitor of MEK/ERK pathways, PD98059, completely abolished the suppressive effect of M-CSF on Bim expression. (C) Transcriptional regulation of *bim* in OCs. No significant change in the mRNA level of three isoforms of *bim*, i.e. bim_{EL}, $_L$ and $_S$ (upper and lower left), or the bim_{EL} specific mRNA level (lower right) was detected in OCs in the presence or absence of M-CSF as determined by RT–PCR (upper) or real-time PCR (lower). The *y*-axis indicates the relative mRNA levels. NS = not significantly different. (D) Effect of adenovirus vector-mediated overexpression of Bim_L and/or Bcl-xL on OC survival. Upper panel: TRAP staining. Lower panel: percentage of OCs surviving. Overexpression of Bim_L promoted apoptosis of OCs ($AxBim_L$). Not only did Bcl-xL overexpression suppress apoptosis of OCs (AxEGFP + AxBcl-xL), but co-expression of Bcl-xL together with Bim_L completely abrogated the pro-apoptotic effect of Bim_L ($AxBim_L$ + AxBcl-xL).

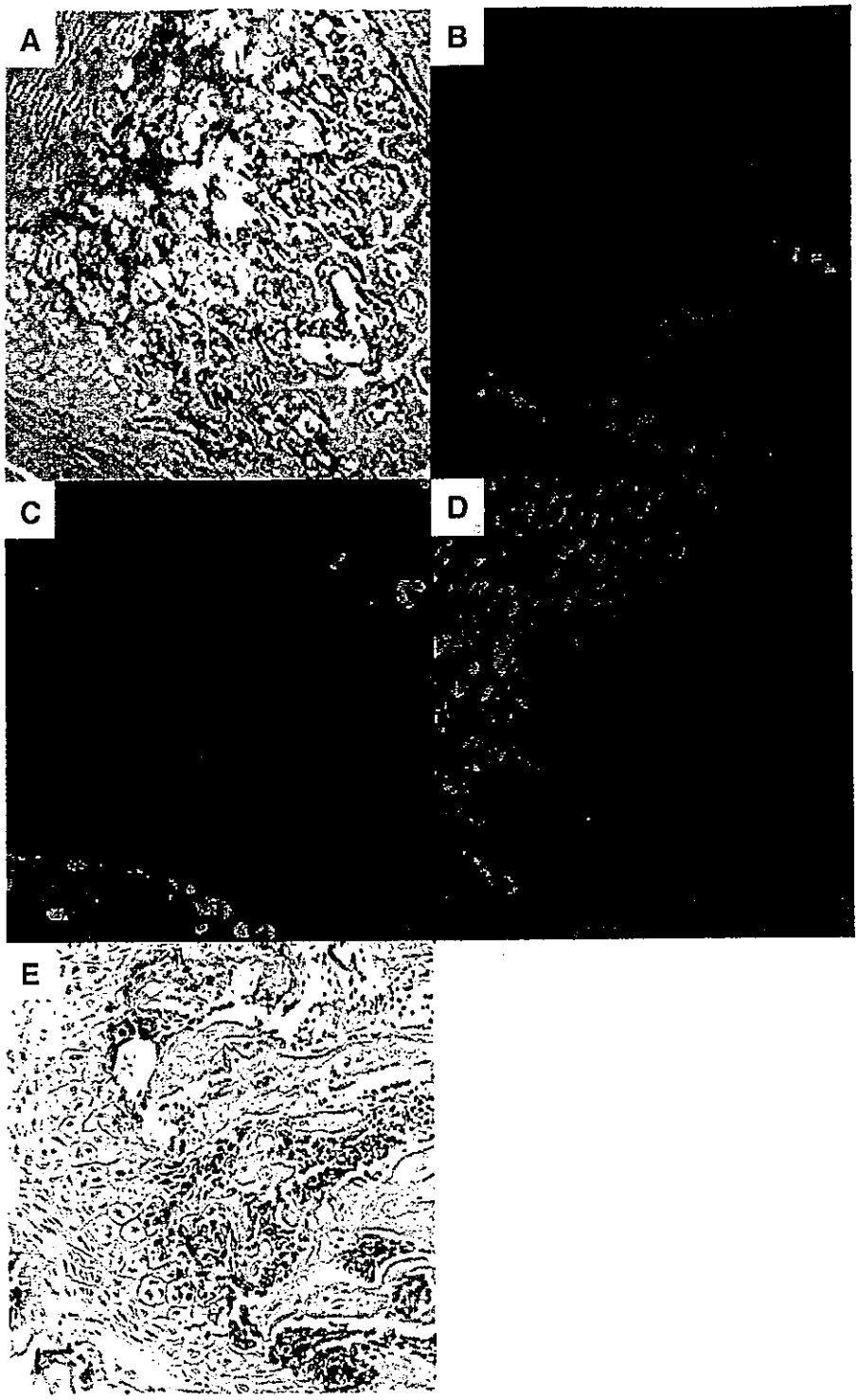

Fig. 2. *In situ* hybridization of the section of the metatarsal bones from a 5-week-old male wild-type mouse using digoxigenin-labeled mouse bim_L (B), procollagen type IA (C) and type II A (D) riboprobes, and TRAP enzymatic staining (A). The labeling was detected by anti-digoxigenin antibody and Alexa 488-labeled anti-rabbit IgG antibody. Note the co-localization of *bim* transcripts with TRAP staining (OCs) (A and B). No positive bim_L staining was co-localized with procollagen type IA staining (osteoblasts) or type IIB staining (chondrocytes). X-gal staining of the tibia from 5-week-old transgenic mice in which *lacZ* gene was introduced into the *bim* locus by homologous recombination also showed the clear positive staining in OCs but not in chondrocytes or osteoblasts (E).

however, remarkably resistant to cytokine withdrawal. Within 48 h of M-CSF depletion, all the wild-type OCs had undergone apoptosis, whereas >90% of *bim*–/– OCs remained alive (Figure 4A).

Interestingly, despite their prolonged survival, *bim*–/– OCs had less bone-resorbing activity than *bim*+/+ cells, as determined by the pit formation assay (Figure 4C). Adenovirus vector-mediated Bim_L expression in *bim*–/– OCs not only reduced their survival, but also recovered bone-resorbing activity of the cells (Figure 4B and C). These results indicate that the skeletal abnormalities in *bim*–/– mice result from impaired activity of OCs.

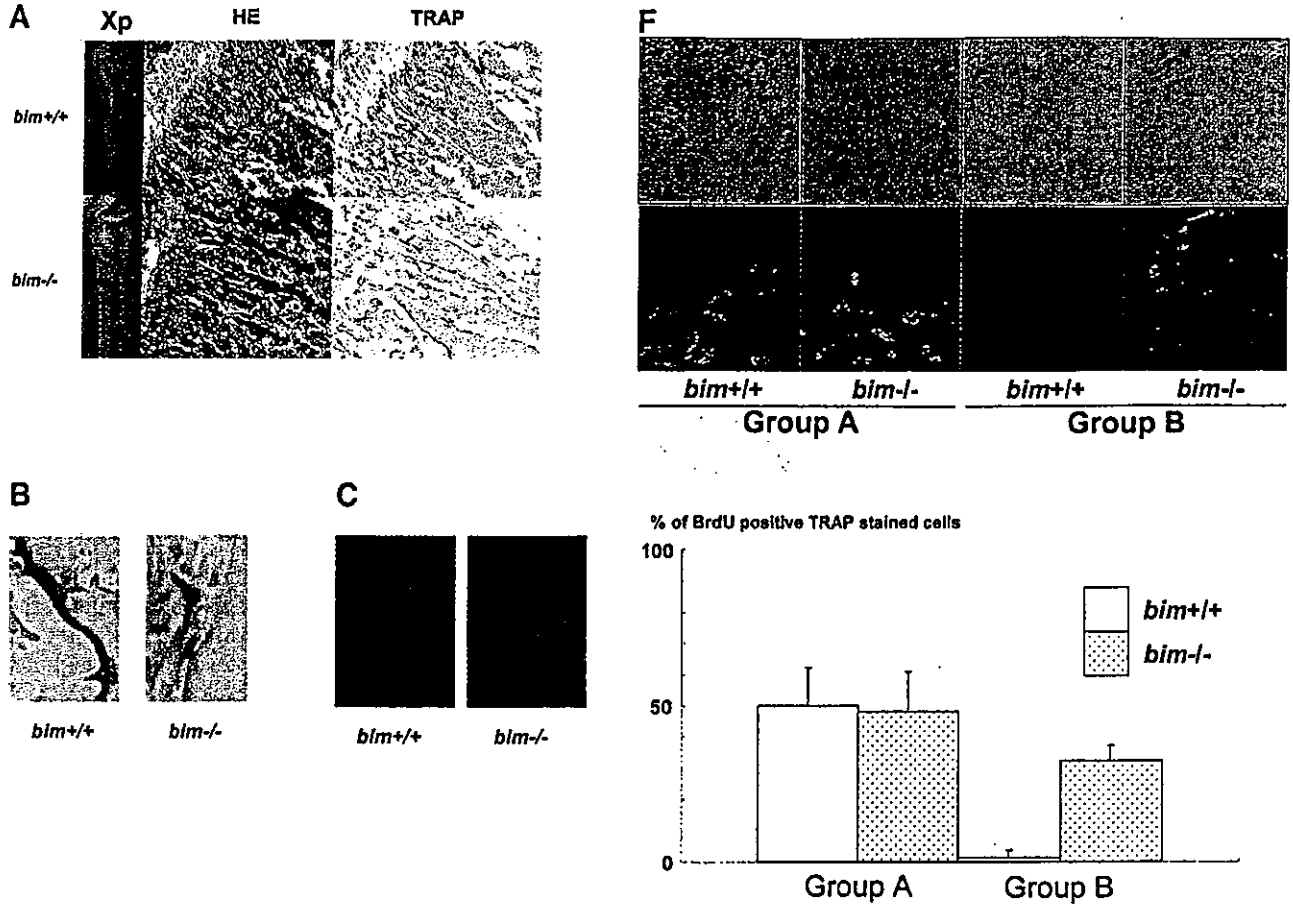

Fig. 3. Bim deficiency causes mild osteosclerosis due to impaired OC activation. (A) Radiological and histological analysis of tibia from 5-week-old *bim+/+* and *bim–/–* male mice (H&E and TRAP staining). *bim–/–* tibia showed expanded secondary spongiosa, exhibiting mild osteosclerosis. (B) *bim–/–* OCs showed smaller and shrunken morphological features compared with *bim+/+* OCs *in vivo* as shown by TRAP staining. (C) Impaired actin ring formation in *bim–/–* OCs. More than 90% of *bim+/+* OCs formed actin rings (left), whereas only 30% of *bim–/–* cells were able to do this (right). (D) Histomorphometric analysis: parameters are measured in the proximal tibia of *bim+/+* and *bim–/–* mice. Data are expressed as means ± SD from five mice of each genotype. BV/TV, trabecular bone volume expressed as a percentage of tibia tissue volume; Tb.Th, trabecular bone thickness; Tb.N, trabecular bone number per mm; Tb.Sp, average space between neighboring trabecular bones; O.Th, osteoid thickness; OS/BS, percentage of bone surface covered by osteoid; Ob.S/BS, percentage of bone surface covered by cuboidal osteoblast; ES/BS, percentage of eroded surface; Oc.N/B.Pm, number of mature OCs per 10 mm of bone perimeter; Oc.S/BS, percentage of bone surface covered by mature OCs. *bim–/–* bones showed reduction of both bone formation markers (O.Th, OS/BS and Ob.S/BS) and bone resorption markers (ES/BS and Oc.S/BS), and increased Oc.N/B/Pm. *&** = significantly different. $*P < 0.005$, $**P < 0.01$. (E) Calcein double labeling of tibia trabecular bone from 13-week-old *bim+/+* (left) and *bim–/–* mice (right). Labeling is visualized by fluorescent microscopy. (F) *bim–/–* OCs have a longer life span *in vivo*. Five-week-old *bim+/+* and *bim–/–* mice ($n = 4$) were fed with water containing 1 mg/ml BrdU for 1 week (labeling period). Mice were then sacrificed either on the next day (group A) or after 6 weeks (group B) of the labeling period, and their tibias were examined by anti-BrdU immunohistochemistry. More than 100 OCs were examined by BrdU immunostaining in the serial sections of the tibia, and the number of BrdU-positive OCs was counted. Fifty percent of *bim+/+* OCs and 48% of *bim–/–* OCs in group A were positively stained by BrdU. However, the proportion of BrdU-positive OCs was markedly reduced to <5% in group B *bim+/+* mice, due to the apoptotic cell death, while >30% of group B *bim–/–* OCs still exhibited BrdU labeling.

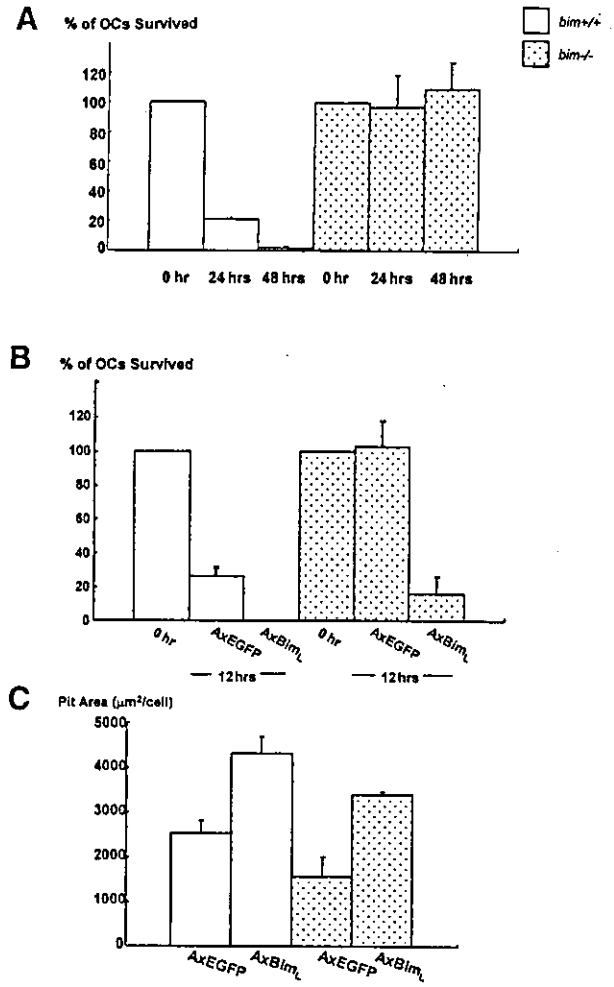

Fig. 4. Effects of Bim on survival and activity of OCs. (A) Survival of *bim+/+* and *bim–/–* OCs. More than 90% of *bim–/–* OCs survived 48 h after M-CSF removal, while all the *bim+/+* OCs had died. (B) Adenovirus vector-mediated Bim_L expression-promoted apoptosis in *bim–/–* OCs as well as in *bim+/+* OCs after 12 h of M-CSF deprivation. (C) Pit-forming activity. The resorption pit area formed by *bim–/–* OCs was significantly less than that formed by *bim+/+* OCs. Overexpression of Bim_L promoted bone-resorbing activity in both *bim+/+* and *bim–/–* OCs.

M-CSF stimulation promotes ubiquitylation-dependent degradation of Bim in OCs

Induction of Bim protein by M-CSF withdrawal (Figure 1A) without changes in mRNA expression levels (Figure 1C) suggested that Bim was regulated post-translationally. Interestingly, treatment of OCs with proteasome inhibitors, such as lactacystin or MG132, greatly enhanced the expression of Bim in OCs even in the presence of M-CSF (Figure 5A). In contrast, MG132 did not affect the expression of other Bcl-2 family members (Figure 5A). This indicates that the ubiquitin–proteasome degradation system is involved in the regulation of Bim expression in these cells. Immunoprecipitation of Bim followed by immunoblot analysis using anti-ubiquitin antibody demonstrated a high level of Bim polyubiquitylation in OCs cultured in MG132, which was greatly enhanced by M-CSF (Figure 5B).

Possible involvement of c-Cbl in ubiquitylation of Bim

The Cbl family proteins are evolutionarily conserved negative regulators of activated tyrosine kinase-coupled receptors, act as E3 ubiquitin ligases, and are involved in OC function (Tanaka *et al.*, 1996; Joazeiro and Weissman, 2000; Sanjay *et al.*, 2001). To determine the role of c-Cbl in the ubiquitylation and degradation of Bim in OCs, we first examined the association of Bim and c-Cbl. GST pull-down experiments showed that recombinant GST–Bim_{EL} fusion protein specifically associated with c-Cbl (Figure 5C, upper panel). c-Cbl was co-immunoprecipitated with Bim in OC lysates in the presence of proteasome inhibitor MG132, and this association was enhanced by M-CSF treatment (Figure 5C, lower panel). Immunofluorescence analysis showed clear co-localization (yellow in Figure 5D, c and d) of Bim and c-Cbl in OCs treated with MG132 and M-CSF. We constructed adenovirus vectors carrying c-Cbl or v-Cbl, which lacks the ubiquitin ligase RING finger domain and acts in a dominant-negative fashion (Taher *et al.*, 2002), and examined their effects on the expression level of Bim in OCs. The upper panel of Figure 5E shows by western blotting with anti-Bim antibody that c-Cbl overexpression (without MG132) reduced Bim expression by increasing Bim ubiquitylation (compare lanes 1 and 5). MG132 treatment increased Bim expression in c-Cbl-overexpressing cells by suppressing proteasomal degradation with or without M-CSF (lanes 7 and 8). In contrast, overexpression of v-Cbl increased the expression of Bim to the maximal level even in the absence of MG132, and the expression was not affected by M-CSF (lanes 9–12). As shown in the lower panel of Figure 5E, overexpression of c-Cbl enhanced Bim ubiquitylation in the absence of M-CSF, and v-Cbl expression suppressed it even in the presence of MG132 and M-CSF.

The role of c-Cbl in M-CSF-dependent ubiquitylation of Bim was confirmed further using OCs generated from c-Cbl–/– mouse bone marrow cells. M-CSF-induced downregulation of Bim was suppressed in c-Cbl–/– OCs as shown by western blotting in Figure 5F. Immunostaining with anti-Bim antibody demonstrated that although no obvious difference in fluorescence intensity was observed between authentic OCs isolated from c-Cbl+/+ and c-Cbl–/– mice, downregulation of Bim by M-CSF treatment was suppressed in c-Cbl–/– OCs (Figure 5G). These results suggest that c-Cbl plays an important role in the ubiquitylation and proteasome-dependent degradation of Bim in OCs.

Stabilization of Bim by lysine mutation reduced the ability of M-CSF to inhibit OC apoptosis

One of the first steps in the ubiquitin–proteasome degradation system includes selective modification of ε-NH_2 groups of lysine residues by ubiquitylation. We constructed retroviral vectors encoding wild-type (wt) or mutated (mt) Bim_{EL}, in which all the ubiquitin acceptor lysine residues (Lys3 and Lys108) are mutated to arginine. These vectors also contained an internal ribosomal entry site (IRES) and enhanced green fluorescent protein (EGFP) to allow identification of infected cells. *bim–/–* OC precursors were infected with either control virus (pMx-IRES-EGFP), pMxBim_{EL}-IRES-EGFP

or pMxmtBim$_{EL}$-IRES-EGFP in the presence of M-CSF and a pan-caspase inhibitor zVAD-FMK. Removal of zVAD-FMK induced rapid apoptosis in the cells expressing mtBimEL within 18 h even in the presence of M-CSF, while almost all of control virus- or 77% of pMx-IRES-Bim$_{EL}$-infected cells survived for at least 24 h. MG132 treatment clearly upregulated the expression of wtBim$_{EL}$, while it did not affect mtBim expression (Figure 6C). Immunoprecipitated mtBim was not ubiquitylated even in the presence of M-CSF and MG132, compared with the wtBim (Figure 6D). These results demonstrate that ubiquitylation and proteasome-mediated degradation are critical regulators of the pro-apoptotic activity of Bim, at least in OCs and their precursors.

Discussion

OCs are terminally differentiated cells with a short life span and, in the absence of trophic factors, such as M-CSF or RANKL, they undergo rapid apoptosis. In the present study, we found that Bim is essential for cytokine withdrawal-induced apoptosis of OCs. Interestingly, although the number of OCs per bone surface was increased and the life span of OCs was elongated in *bim–/–* mice, these animals had mild osteosclerosis due to the low turnover of the skeletal tissues. This phenotype appears to be due to abnormalities in OCs because they are the only relevant cell type in skeletal tissues that express Bim. Moreover, experiments in tissue culture demonstrated that in spite of the retarded apoptosis of *bim–/–* OCs, bone-resorbing activity was significantly reduced compared with *bim+/+* OCs. Adenovirus vector-mediated restoration of Bim$_L$ expression in *bim–/–* OCs not only promoted cytokine withdrawal-induced apoptosis but also upregulated their bone-resorbing activity. Our results are reminiscent of previous studies by Roodman and co-workers, which showed that OC-specific overexpression of Bcl-xL and SV40 large T antigen under the control of TRAP promoter in transgenic mice induced osteosclerosis although OC apoptosis was markedly reduced in the animals (Hentunen *et al.*, 1998). These results suggest that the balance between Bim and anti-apoptotic Bcl-2 family members, such as Bcl-2 and Bcl-xL, is critical for normal skeletal homeostasis. The molecular mechanism of reduced bone-resorbing activity in *bim–/–* OCs still remains unclear. Several previous studies demonstrated that although M-CSF promotes the survival of OCs, it rather suppresses their bone-resorbing activity (Hattersley *et al.*, 1988; Fuller *et al.*, 1993; Miyazaki *et al.*, 2000). M-CSF induces cytoskeletal reorganization of OCs and enhances their migration and chemotaxis, and motile OCs are non-polarized cells with low bone-resorbing activity. Because M-CSF strongly suppressed Bim expression in OCs, we speculate that *bim* deficiency somehow mimics M-CSF treatment, which may explain the reduced bone-resorbing activity of the cells. Alternatively, aged OCs that have already engorged a lot of bone become exhausted, making it difficult to resorb more bone, and the presence of aged OCs suppresses the beginning of the new bone remodeling cycle. Further studies are required to clarify further the molecular mechanism of the reduced bone resorption of *bim–/–* OCs and the osteosclerosis in *bim–/–* mice.

Recently, the role of ubiquitylation in regulating apoptosis has been widely recognized and attracted a great deal of interest (Jesenberger and Jentsch, 2002). For example, p53, which is essential for DNA damage-induced apoptosis in many cell types, is degraded by the ubiquitin–proteasome pathways (Haupt *et al.*, 1997; Kubbutat *et al.*, 1997). Moreover, inhibitor of apoptosis proteins (IAPs) (e.g. XIAP, cIAP1 and cIAP2), which can bind and neutralize initiator and/or effecter caspases, contain RING finger domains, and promote their auto-ubiquitylation and proteasome-mediated degradation when cells are exposed to apoptotic stimuli (Yang *et al.*, 2000). Dephosphorylation and subsequent ubiquitylation-dependent degradation of Bcl-2 was reported to be involved in TNF-α-induced apoptosis of endothelial cells (Dimmeler *et al.*, 1999). Finally, proteasome-dependent degradation of the BH3-only proteins Bid (tBid) and Bik has been reported in HeLa cells and leukemia-derived cells, respectively (Breitschopf *et al.*, 2000; Marshansky *et al.*, 2001). Previous studies have revealed that Bim can be regulated at the transcriptional level in hemopoietic progenitors and neurons (Putcha *et al.*, 2001; Shinjyo *et al.*, 2001; Whitfield *et al.*, 2001; Dijkers *et al.*, 2002), and the regulation of Bim activity by phosphorylation by ERK and/or JNK has been reported (Biswas and Greene, 2002; Lei and Davis, 2003; Weston *et al.*, 2003). Very recently, the ubiquitylation of Bim and its upregulation by proteasome inhibitors were reported (Ley *et al.*, 2003). However, the physiological function of such a modification, especially in primary cells, has not been established. We demonstrate here that Bim ubiquitylation is regulated by M-CSF in OCs, and this modification plays a critical role in their survival. In M-CSF-stimulated cells, Bim is ubiquitylated and its expression kept at low levels by proteasomal degradation. After cytokine withdrawal, Bim protein levels are rapidly increased due to the reduced ubiquitylation and degradation. Bim is associated with c-Cbl in OCs, and overexpression of c-Cbl suppressed the expression of Bim in OCs by promoting its ubiquitylation, while that of v-Cbl, which acts in a dominant-negative fashion, increased the Bim level even in the presence of M-CSF, suggesting the important role of c-Cbl in Bim ubiquitylation. This was confirmed further using OCs from c-Cbl–/– mice (Figure 5F and G).

The critical role of ubiquitylation and proteasome-mediated degradation in regulating the pro-apoptotic activity of Bim was proven by showing that a mutant of Bim$_{EL}$ that cannot be ubiquitylated can kill OCs even in the presence of M-CSF, whereas wtBim$_{EL}$ can be kept in check by cytokine receptor signaling. We found that MEK1^{CA} introduction downregulates Bim expression in OCs, and a specific inhibitor of MEK/ERK pathways, PD98059, abolished the effect of M-CSF (Figure 5B), indicating that ERK signaling mainly promotes Bim ubiquitylation. This suggests that the state of phosphorylation of Bim may be important for its ubiquitylation, or that E3 ubiquitin ligation to Bim is regulated mainly by ERK pathways. The detailed mechanism of Bim ubiquitylation still remains elusive.

Targeted disruption of *bim* induced the accumulation of myeloid and lymphoid cells, and perturbation of T-cell development, and caused autoimmune disorders (Bouillet *et al.*, 1999, 2002; Villunger *et al.*, 2003). Bim is also

involved in the apoptosis of neurons (Putcha *et al.*, 2001; Whitfield *et al.*, 2001), and we found that it plays an essential role in regulating the survival and bone-resorbing activity of OCs. There is substantial evidence that abnormalities in the ubiquitylation/proteasome degradation machinery can cause diseases, such as neurodegenerative diseases, cancers and autoimmune diseases (Glickman and Ciechanover, 2002). Therefore, the failure in the ubiquitin–proteasome-dependent degradation of Bim may cause various abnormalities in the skeletal homeostasis, the immune systems and neuronal systems. Further studies are required to elucidate the mechanism of action and the regulation of Bim, and the role of Bim in skeletal disorders.

Materials and methods

Antibodies and chemicals

Antibodies to Bid and Bax were purchased from Cell Signaling Technology (Beverly, MA). Antibodies to Bim (M-20 for immunoprecipitation), Bcl-xL, ubiquitin and c-Cbl were from Santa Cruz Technology (Santa Cruz, CA), and antibodies to Bim (for western blotting) were from BD Biosciences Pharmingen (San Jose, CA). Antibody to Bim (for immunocytochemistry) was from Oncogene Research Products (Cambridge, MA). Recombinant mouse M-CSF was

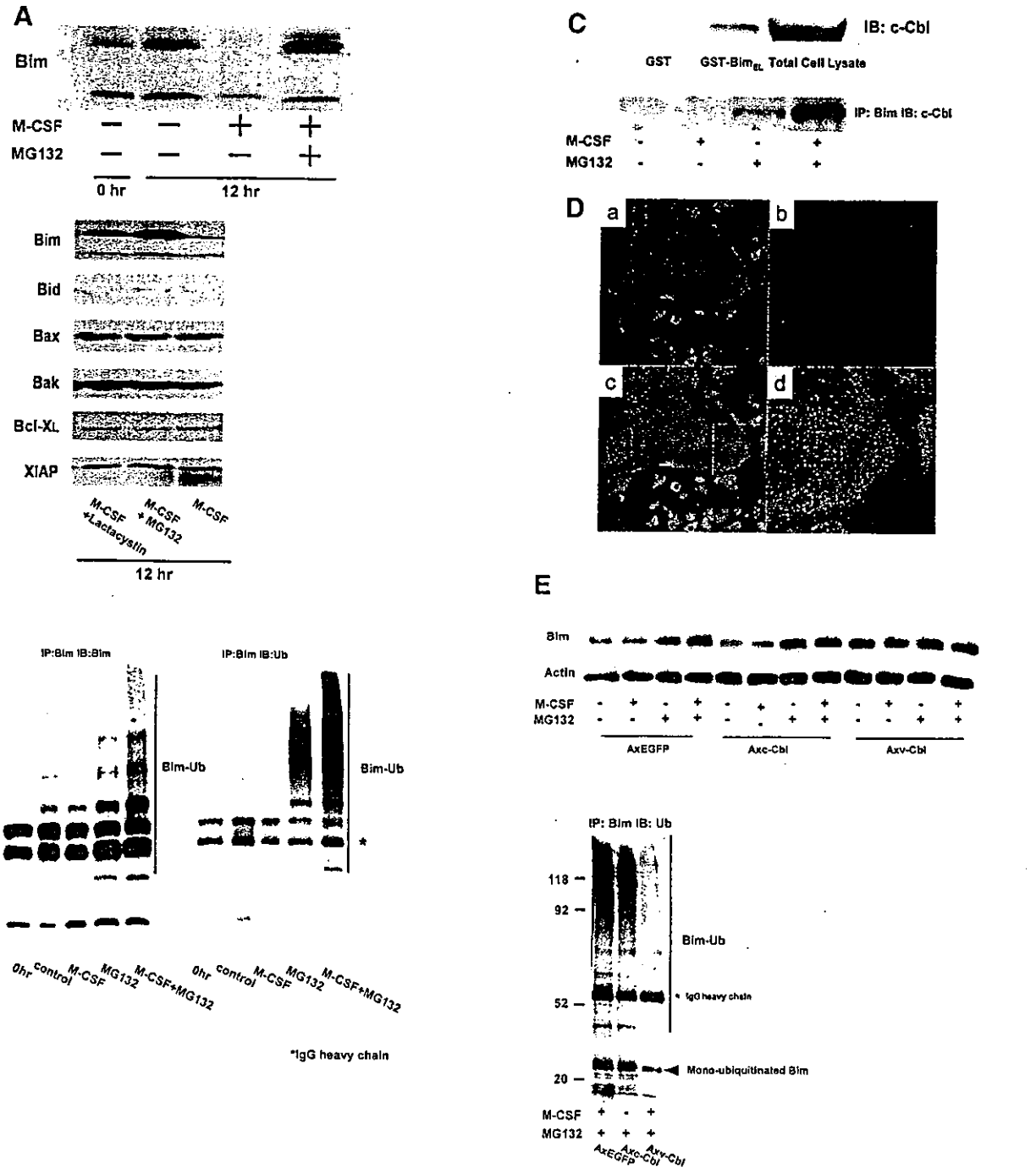

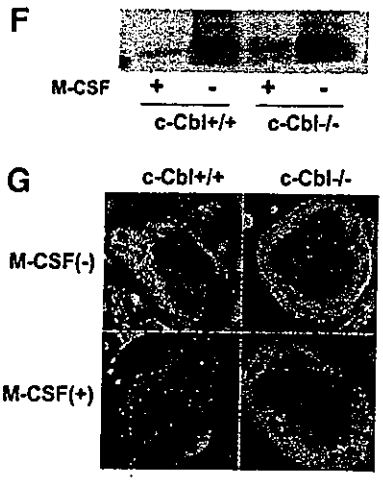

Fig. 5. Ubiquitylation-dependent degradation of Bim in OCs. (**A**) Western blotting. Upper panel: Bim protein level increased after 12 h of osteoblast removal, which was suppressed in the presence of M-CSF. MG132 treatment strongly upregulated Bim expression even in the presence of M-CSF. Lower panel: no obvious upregulation or downregulation of Bid, Bax, Bak, Bcl-xL and XIAP level was induced by MG132 or lactacystin. (**B**) Ubiquitylation of Bim in OCs. Proteins immunoprecipitated with anti-Bim antibody were immunoblotted with an anti-Bim antibody (left) or an anti-ubiquitin antibody (right). Ubiquitylated Bim was detected as upper-shifted bands in both anti-Bim and anti-ubiquitin blotting (Bim-Ub). Ubiquitylated Bim was detected when cells were treated with MG132, and marked enhancement of its ubiquitylation was induced by M-CSF treatment. (**C**) Association of c-Cbl with Bim in OCs. Upper panel: cell lysates of M-CSF-treated OCs were incubated with bacterially expressed GST–Bim_{EL} fusion protein, and association with c-Cbl was determined by western blotting. c-Cbl was associated with GST–Bim_{EL} but not with GST. Lower panel: Bim was immunoprecipitated from OC cell lysates, and its association with c-Cbl was examined by western blotting. Co-immunoprecipitation of c-Cbl with Bim was observed in MG132-treated OCs, which was enhanced by M-CSF treatment. (**D**) Double immunofluorescence of (a) Bim (green) and (b) c-Cbl (red) in authentic OCs isolated from normal mice. Co-localization of these two molecules (yellow in c and d) was observed in the presence of MG132 and M-CSF. (d) An enlargement of the rectangular area in (c). (**E**) Involvement of c-Cbl in the ubiquitylation of Bim in OCs. Upper panel: adenovirus vector-mediated overexpression of c-Cbl (Axc-Cbl) decreased the protein level of Bim in OCs in the absence of M-CSF (compare lanes 1 and 5). MG132 treatment increased Bim expression in c-Cbl-overexpressing cells with or without M-CSF (lanes 7 and 8). On the other hand, adenovirus vector-induced overexpression of v-Cbl (Axv-Cbl) increased Bim expression even in the absence of MG132, which was not affected by M-CSF treatment (lanes 9–12). Lower panel: Bim was immunoprecipitated and immunoblotted with anti-ubiquitin antibody. c-Cbl-overexpressing OCs showed Bim ubiquitylation in the absence of M-CSF (lane 2) to a similar extent as in EGFP virus-infected OCs treated with M-CSF (lane 1). v-Cbl overexpression suppressed Bim ubiquitylation even in the presence of MG132 and M-CSF (lane 3). (**F**) M-CSF-induced downregulation of Bim was suppressed in c-Cbl–/– OCs. OCs generated from bone marrow cells of c-Cbl–/– mice (c-Cbl–/–) or their normal littermates (c-Cbl+/+) were treated or not with M-CSF. Western blotting with anti-Bim antibody demonstrates that although no difference in Bim level was observed between c-Cbl+/+ and c-Cbl–/– OCs in the absence of M-CSF (lanes 2 and 4, respectively), M-CSF-induced downregulation of Bim was suppressed in c-Cbl–/– OCs (lane 3). (**G**) Immunofluorescence of primary OCs with anti-Bim antibody. Primary OCs isolated from c-Cbl+/+ and c-Cbl–/– mice were cultured in the presence or absence of M-CSF (10 ng/ml) for 12 h, and immunostained with anti-Bim antibody. Although no apparent difference in fluorescence intensity was observed between c-Cbl+/+ and c-Cbl–/– OCs in the absence of M-CSF, M-CSF-induced downregulation was scarcely detected in c-Cbl–/– OCs.

bought from TECHNE Co. (Minneapolis, MN) and soluble RANKL was from Wako Pure Chemical Co. (Osaka, Japan). α-Modified minimum essential medium (αMEM) was purchased from Gibco-BRL, Life Technologies Inc. (Rockville, MD), and fetal bovine serum (FBS) was from Sigma (St Louis, MO). Bacterial collagenase was purchased from Wako Pure Chemical Co. (Osaka, Japan), $1\alpha,25(OH)_2D_3$ from Calbiochem (La Jolla, CA) and dispase from Godoshusei (Tokyo, Japan). The broad-spectrum caspase inhibitor zVAD-FMK was from Calbiochem. Other chemicals and reagents used in this study were of analytical grade.

Expression constructs and gene transduction

The recombinant adenovirus vectors were constructed as previously described (Miyazaki *et al.*, 2000; Mochizuki *et al.*, 2002; Yamaguchi *et al.*, 2003). Adenovirus infection of OCs was performed as previously reported (Tanaka *et al.*, 1998; Miyazaki *et al.*, 2003). Retroviral vectors, pMx-Bim_{EL}-IRES-EGFP and pMx-mtBim_{EL}-IRES-EGFP, were constructed by inserting full-length mouse cDNA of bim_{EL} and mutated bim_{EL}, in which the two ubiquitin acceptor lysine residues (Lys3 and Lys108) were mutated to arginine, into pMx-IRES-EGFP vector. Retrovirus packaging was performed by transfection of the pMx vectors into BOSC cells. Retrovirus infection of OC precursors was carried out as previously described (Kobayashi *et al.*, 2001).

Animals, cells and cultures

Newborn and 8-week-old male ddY mice were purchased from Shizuoka Laboratories Animal Center (Shizuoka, Japan). The breeding and genotyping of *bim–/–* mice (on a C57BL/6 N>12 genetic background) was performed as previously described (Bouillet *et al.*, 1999). The transgenic mice in which a reporter *lacZ* gene was introduced into the *bim* locus was generated by homologous recombination. c-Cbl–/– mice were generated and identified as previously reported (Naramura *et al.*, 1998). Authentic OCs were obtained from the long bones of 2- to 4-day-old neonatal mice as reported (Chiusaroli *et al.*, 2003). To obtain large numbers of cells for biochemical analyses, we utilized the co-culture system established by Takahashi *et al.* (1988).

Immunoblotting and immunoprecipitation

Immunoblotting and immunoprecipitation were performed as previously reported (Tanaka *et al.*, 1998).

Immunofluorescence

Cells cultured on glass coverslips were fixed in 3.7% (v/v) formaldehyde in phosphate-buffered saline (PBS) for 10 min, and then washed three times in PBS. Cells were permeabilized in 0.05% saponin for 30 min, blocked in 5% normal goat serum (Boehringer) for 30 min, incubated in appropriate primary antibodies, washed in PBS, incubated with fluorescein-conjugated secondary antibody, and finally washed in PBS and mounted in FluorSave. Cells were examined using a confocal imaging system (MRC-600; Bio-Rad Laboratories).

GST fusion proteins

A pGEX plasmid containing the GST–Bim_{EL} was used to transform *Escherichia coli* B21 cells (Life Technologies, Inc.). After induction of protein expression with 0.1 μM isopropyl-1-thio-β-D-galactopyranoside (Sigma) for 2–4 h, the bacteria were resuspended in a lysis buffer containing 50 mM Tris–HCl, pH 8.0, 100 μM NaCl, 1 mM phenylmethylsulfonyl fluoride (PMSF) and 1% Triton X-100 and were disrupted further by sonication. Following centrifugation at 10 000 *g* for 20 min, the induced proteins were adsorbed to bead-immobilized glutathione. Soluble GST fusion proteins were obtained by elution with 2 mM reduced glutathione in 50 mM Tris–HCl pH 8.0. For *in vitro* binding assays, bead-adsorbed GST or GST fusion proteins (5 μg/sample) were incubated with OC cell lysates at 4°C on a rotator for 3 h. The beads were then washed three times with lysis buffer, and bound proteins were subjected to SDS–PAGE under reducing conditions followed by immunoblotting.

RT–PCR and real-time PCR

mRNAs was isolated from OCs, and reverse-transcribed by the Super Script First-Strand Synthesis system for RT–PCR (Invitrogen), according to the manufacturer's protocol. The primers we utilized to detect *bim* and *gapdh* were as follows: *bim*, 5′-ATGGCCAAGCAACCTTCTGA and 3′-TCAATGCCTTCTCCATACCAG; *gapdh*, 5′-GTATGTCGTGGAGT-CTACTGGTGT and 3′-TACTCCTTGGAGGCCATGTAGGCC. The primers utilized to detect *bax* and *bcl-xL* were as previously reported by Okahashi *et al.* (1998). Reverse-transcribed mRNAs were analyzed by the ABI Prism® 7000 Sequence Detection System (Applied Biosystems,

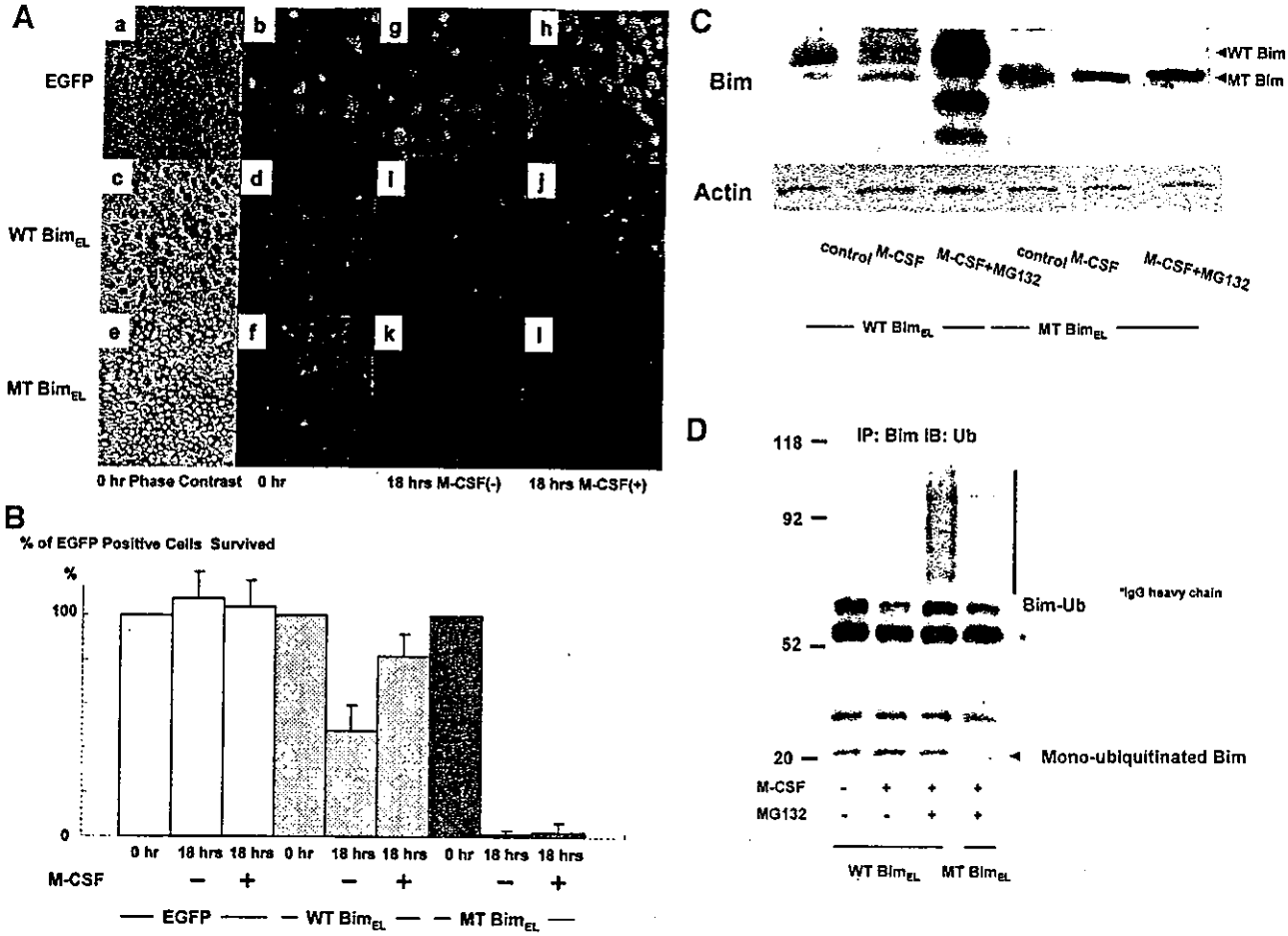

Fig. 6. Effect of mutations in Bim that prevent ubiquitylation. (A) Phase contrast (a, c and e) and immunofluorescence microscopy: *bim–/–* bone marrow cells cultured in the presence of M-CSF (100 ng/ml) and zVAD-FMK (100 μM) were infected with either pMx-IRES-EGFP, pMxBim$_{EL}$-IRES-EGFP or pMxmtBim$_{EL}$-IRES-EGFP. After 7 days of the retrovirus infection, when gene expression was confirmed by EGFP fluorescence (b, d and f), cultures were deprived of zVAD-FMK. At 18 h after zVAD-FMK removal, most of pMx-IRES-EGFP- and pMxBim$_{EL}$-IRES-EGFP-infected cells survived as identified by EGFP fluorescence (h and j), compared with the survival rate of 5% in pMxmtBim$_{EL}$-IRES-EGFP virus-infected cells (l). Both pMxBim$_{EL}$-IRES-EGFP- and pMxmtBim$_{EL}$-IRES-EGFP-infected cells died when M-CSF was removed from the cultures (i and k). (B) The survival ratio of EGFP-positive cells. Almost 100% of the control cells survived even 18 h after z-VAD-FMK removal in the presence of M-CSF. At 18 h after zVAD-FMK removal, almost 100% of pMx-IRES-EGFP- and >70% of pMxBim$_{EL}$-IRES-EGFP-infected cells survived as identified by EGFP fluorescence (EGFP and WTBim$_{EL}$), compared with the survival rate of 5% in pMxmtBim$_{EL}$-IRES-EGFP virus-infected cells (MTBim$_{EL}$). (C) The proteasome inhibitor MG132 enhanced the expression level of wtBim in pMxBim$_{EL}$-IRES-EGFP-infected OC precursors (WTBim) even in the presence of M-CSF, while no obvious upregulation of MTBim was observed in pMxmtBim$_{EL}$-IRES-EGFP infected cells (MTBim). (D) WTBim or MTBim was immunoprecipitated from cell lysates of pMxBim$_{EL}$-IRES-EGFP-infected (WTBim$_{EL}$) or pMxmtBim$_{EL}$-IRES-EGFP-infected cells (MTBim$_{EL}$) using anti-Bim polyclonal antibody, and the immunoprecipitates were immunoblotted with anti-ubiquitin antibody. Treating the cells with the proteasome inhibitor MG132 strongly increased the ubiquitylation of Bim, while no ubiquitylation of mtBim was observed.

CA). The primers we utilized in real-time PCR to detect the common form of all *bim* splice variants and the *bim$_{EL}$*-specific form were as follows: *bim* common form, 5′-CTTCCATACGACAGTCTC and 3′-AACCATTTGAGGGTGGTCTTC; *bim$_{EL}$*-specific form, 5′-GTCCTC-CAGTGGGTATTTCT and 3′-CAGATCTTCAGGTTCCTCCT.

In situ hybridization

In situ hybridization was performed as described previously (Lee *et al.*, 1995) by using complementary digoxigenin-labeled riboprobes for mouse *bim$_L$*, procollagen type IA and procollagen type IIA.

Histomorphometry

Histomorphometric analysis of proximal tibia from *bim+/+* and *bim–/–* littermates was performed as previously described (Akune *et al.*, 2002).

Survival of OCs

The survival of OCs was measured as previously reported (Miyazaki *et al.*, 2000). Cell survival is expressed as the percentage of morphologically intact TRAP-positive multinucleated cells. Other cultures were incubated further for the indicated times, and then the number of living OCs was counted. The number of viable cells remaining at the different time points is shown as a percentage of the cells at the start of the experiment.

Pit formation assay

The pit formation assay was performed as previously described (Tanaka *et al.*, 1998). The resorbed area was measured using an image analysis system (SYSTEM SUPPLY, Nagano, Japan) linked to a light microscope (Nikon, Tokyo, Japan).

Statistical analysis

Each series of experiments was repeated at least three times. The results obtained from a typical experiment were expressed as the means ± SD. Significant differences were determined using factorial analysis of variance.

Acknowledgements

The authors thank R.Yamaguchi and M.Ikeuchi (Department of Orthopaedic Surgery, The University of Tokyo), L.Neff (Yale University) and M.Robati (WEHI) for expert technical assistance,